Flavor origin of dark matter and its relation with leptonic nonzero θ_{13} and Dirac CP phase δ

Subhaditya Bhattacharya[a,1], Biswajit Karmakar[a,2], Narendra Sahu[b,3], Arunansu Sil[a,4]

[a] *Department of Physics, Indian Institute of Technology Guwahati, 781039 Assam, India,*
[b] *Department of Physics, Indian Institute of Technology, Hyderabad, Kandi, Sangareddy 502285, Medak, Telengana, India*

Abstract

We propose a minimal extension of the standard model by including a $U(1)$ flavor symmetry to establish a correlation between the relic abundance of dark matter, measured by WMAP and PLANCK satellite experiments and non-zero value of $\sin\theta_{13}$ observed at DOUBLE CHOOZ, Daya Bay, RENO and T2K. The flavour symmetry is allowed to be broken at a high scale to a remnant $\mathcal{Z}_2$ symmetry, which not only ensures the stability to the dark matter, but also gives rise to a modification to the existing A_4-based tri-bimaximal neutrino mixing. This deviation in turn suggests the required non-zero value of $\sin\theta_{13}$. We assume the dark matter to be neutral under the existing A_4 symmetry while charged under the $U(1)$ flavor symmetry. Hence in this set-up, the non-zero value of $\sin\theta_{13}$ predicts the dark matter charge under $U(1)$, which can be tested at various ongoing and future direct and collider dark matter search experiments. We also point out the involvement of nonzero leptonic CP phase δ, which plays an important role in the analysis.

[1] subhab@iitg.ernet.in
[2] k.biswajit@iitg.ernet.in
[3] nsahu@iith.ac.in
[4] asil@iitg.ernet.in

1 Introduction

After the Higgs discovery at the LHC, the standard model (SM) of particle physics seems to be complete. However, it does not explain many current issues in particle physics which are supported by experiments. In particular, the oscillation experiments [1] confirm that the neutrinos are massive and they mix with each other. Contrary to this finding, neutrinos are massless within the framework of SM. Another outstanding problem in particle physics as of today is the nature of dark matter (DM), whose relic abundance is precisely measured by the WMAP [13] and PLANCK [14] satellite experiments to be $0.094 \leq \Omega_{\rm DM}h^2 \leq 0.130$. In fact, the existence of DM is strongly supported by the galactic rotation curve, gravitational lensing and large scale structure of the Universe [12] as well. However, the SM of particle physics fails to provide a candidate of DM. In this work our aim is to go beyond the SM of particle physics to explore scenarios which can accommodate a candidate of DM as well as non-zero neutrino masses and mixings.

Flavor symmetries are often used to explore many unsolved issues within and beyond the SM of particle physics. For example, a global $U(1)$ flavor symmetry was proposed a long ago to explain the quark mass hierarchy and Cabibbo mixing angle [2]. Subsequently many flavor symmetric frameworks have been adopted to explain neutrino masses and mixings in the lepton sector. In particular, a tri-bimaximal (TBM) lepton mixing generated from a discrete flavor symmetry such as A_4 attracts a lot of attention [3, 4] due to its simplicity and predictive nature. However the main drawback of these analyses was that it predicts vanishing reactor mixing angle θ_{13} which is against the recent robust observation of $\theta_{13} \approx 9^\circ$ [5, 6, 7] by DOUBLE CHOOZ [8], Daya Bay [9], RENO [10] and T2K [11] experiments. Hence, a modification of the TBM structure of lepton mixing is required.

In this work we consider the existence of a dark sector [16] consisting of vector-like fermions which are charged under an additional $U(1)$ flavor symmetry. Specifically, we consider a vector-like SM singlet fermion (χ^0) and a $SU(2)_L$ doublet fermion (ψ) which are odd under the remnant $\mathcal{Z}_2$ symmetry generated from the broken $U(1)$. The neutral components mix to give rise a fermionic DM (ψ_1). Note that in the simplest case, a singlet fermion (χ^0) can generate a Higgs portal interaction by dimension five operator suppressed by the new physics scale as $(\overline{\chi^0}\chi^0 H^\dagger H)/\Lambda$. However, as we argue, that the new physics scale (Λ) involved in the theory has to generate the required neutrino mass as well and thus making it very high. As a result, the annihilation rate of DM becomes too small which in turn make the relic density over abundant. On the other hand, a vector-like fermion doublet (ψ) suffers from a large annihilation cross-section to SM through Z mediation and is never enough to produce the required density. It is only through the mixing of these two that can produce correct relic density as we demonstrate here. We also assume the existence of a TBM neutrino mixing pattern (in a basis where charged leptons are diagonal) based on A_4 symmetry. The interaction between the dark and the lepton sector of the SM is mediated by flavon fields charged under the $U(1)$ and/or A_4. These flavons also take part in producing additional interactions involving lepton and Higgs doublets. The $U(1)$ symmetry, once allowed to be broken by the vacuum expectation value (vev) of a flavon, generates a non-zero $\sin\theta_{13}$ after the electroweak symmetry breaking (and when A_4 breaks too). We show that the non-zero value of $\sin\theta_{13}$ is proportional to the strength of Higgs portal coupling of DM giving rise to the correct relic density. In other words, the precise value of $\sin\theta_{13}$ and DM relic density can fix the charge of dark matter under $U(1)$ flavor symmetry. Indeed it is true for the Dirac CP violating phase $\delta = 0$ as shown in our previous work [18]. However, we have found here that the non-zero values of δ plays an important role for the determination of DM charge under $U(1)$ flavor symmetry. Although the current allowed range of δ ($0^\circ - 360^\circ$) can significantly increase the uncertainty in the determination of DM flavor charge (compared to $\delta = 0$ scenario), a future measurement of δ would be important in fixing the charge. In [18], we have assumed a prevailing TBM pattern and here in this work we provide an explicit construction of that too. We also show that the effective Higgs portal coupling of the vector-like leptonic DM can be tested at future direct search experiments, such as Xenon1T [15] and at the Large Hadron Collider (LHC) [16, 17].

The draft is arranged as follows. In section 2 we discuss the relevant model for correlating non-zero $\sin\theta_{13}$ to Higgs portal coupling of DM which gives correct relic density. In section 3 and 4, we obtain the constraints on model parameters from neutrino masses and mixing and relic abundance of dark matter

respectively. In section 5, we obtain the correlation between the non-zero $\sin\theta_{13}$ and Higgs portal coupling of dark matter and conclude in section 6.

2 Structure of the model

In this section, we describe the field content and symmetries involved. We consider an effective field theory approach for realizing the neutrino masses and mixing while trying to connect it with the DM sector as well. The set-up includes the interaction between these two sectors which has the potential to generate adequate θ_{13}, and hence a deviation of TBM mixing happens, to match with the experimental observation while satisfying the constraints from relic density and direct search of DM.

2.1 Neutrino Sector

Field	e_R	μ_R	τ_R	ℓ	H	ψ	χ^o	ϕ_S	ϕ_T	ξ	η	ϕ
$SU(2)_L$	1	1	1	2	2	2	1	1	1	1	1	1
A_4	1	$1''$	$1'$	3	1	1	1	3	3	1	$1'$	1
Z_3	ω	ω	ω	ω	1	1	1	ω	1	ω	ω	1
Z_2	-1	-1	-1	1	1	-1	-1	1	-1	1	1	1
$U(1)$	0	0	0	0	0	q_1	q_2	0	0	0	$-x$	x

Table 1: Fields content and transformation properties under the symmetries imposed on the model. Here $nx = q_1 - q_2$ (justified from Eq.(8)), n will be determined later.

The basic set-up relies on the A_4 symmetric construction of the Lagrangian associated with neutrino mass term [3, 4]. Based on the construction by Altarelli-Feruglio (AF) model [4] (for generating TBM mixing), we have extended the flavon sector and symmetry of the model. The SM doublet leptons (ℓ) transform as triplet under the A_4 symmetry while the singlet charged leptons: e_R, μ_R and τ_R transform as $1, 1^{''}$ and $1^{'}$ respectively under A_4. The flavon fields and their charges (along with the SM fields) are described in Table 1. The flavons ϕ_S, ϕ_T and ξ break the A_4 flavor symmetry by acquiring vevs in suitable directions. Note that here ϕ_S and ϕ_T transform as A_4 triplets but the flavon ξ and the SM Higgs doublet (H) transform as a singlet under A_4. So the contribution to the effective neutrino mass matrix coming through the higher dimensional operator respecting the symmetries considered can be written as

$$-\mathcal{L}_{\nu_0} = (\ell H \ell H)(y_1\xi - y_2\phi_S)/\Lambda^2\,, \tag{1}$$

where Λ is the cut off scale of the theory and y_1, y_2 represents respective coupling constant. The scalar fields break the flavor symmetry when acquire vevs along $\langle\phi_S\rangle = (v_S, 0, 0)$, $\langle\phi_T\rangle = v_T(1,1,1)$, $\langle\xi\rangle = v_\xi$ and $\langle H\rangle = v$. As a result we obtain the light neutrino mass matrix as

$$(m_\nu)_0 = \begin{pmatrix} a - 2b/3 & b/3 & b/3 \\ b/3 & -2b/3 & a + b/3 \\ b/3 & a + b/3 & -2b/3 \end{pmatrix}, \tag{2}$$

where $a = y_1(v^2/\Lambda)\epsilon$ and $b = y_2(v^2/\Lambda)\epsilon$, with $\epsilon = v_\xi/\Lambda = v_S/\Lambda$ is considered without loss of generality as any prefactor (due to the mismatch of vevs) can be absorbed in the definition of y_2. The above mass matrix can be diagonalized by the TBM mixing matrix matrix [19]

$$U_{TB} = \begin{pmatrix} \sqrt{\frac{2}{3}} & \frac{1}{\sqrt{3}} & 0 \\ -\frac{1}{\sqrt{6}} & \frac{1}{\sqrt{3}} & -\frac{1}{\sqrt{2}} \\ -\frac{1}{\sqrt{6}} & \frac{1}{\sqrt{3}} & \frac{1}{\sqrt{2}} \end{pmatrix}. \tag{3}$$

The relevant contribution to charged leptons (considering charges from Table 1) can be obtained via

$$\mathcal{L}_l = \frac{y_e}{\Lambda}(\bar{\ell}\phi_T)He_R + \frac{y_\mu}{\Lambda}(\bar{\ell}\phi_T)'H\mu_R + \frac{y_\tau}{\Lambda}(\bar{\ell}\phi_T)''H\tau_R\,, \tag{4}$$

which yields the diagonal mass matrix:

$$M_l = \begin{pmatrix} y_e v\frac{v_T}{\Lambda} & 0 & 0 \\ 0 & y_\mu v\frac{v_T}{\Lambda} & 0 \\ 0 & 0 & y_\tau v\frac{v_T}{\Lambda} \end{pmatrix}. \tag{5}$$

Note that this is the leading order contribution (and is proportional to $1/\Lambda$) in the charged lepton mass matrix. Due to the symmetry of the model as described in Table 1 (including the $U(1)$ symmetry to be discussed later) there will be no term proportional to $1/\Lambda^2$. Therefore no contribution to the lepton mixing matrix originated from the charged lepton sector upto $1/\Lambda^2$ is present. Here it is worthy to mention that the dimension-5 operator $\ell H\ell H/\Lambda$ is forbidden due to the Z_3 symmetry specified in Table 1. This additional symmetry also forbids the dimension-6 operator $\ell H\ell H(\phi_T+\phi_T^\dagger)/\Lambda^2$. The $U(1)$ flavor symmetry considered here does not allow terms involving ϕ, η (such as: $\ell H\ell H(\phi+\eta)/\Lambda^2$) as discussed (where ϕ and η are charged under $U(1)$ but the SM particles are not). Therefore, Eq. (1) is the only relevant term up to $1/\Lambda^2$ order contributing to the neutrino mass matrix $(m_\nu)_0$ ensuring its TBM structure as in Eq. (2). Note that these kind of structure of the neutrino mass matrix of $(m_\nu)_0$ can also be obtained in a A_4 based set-up either in a type-I, II or inverse seesaw framework [20, 21, 22, 23].

The immediate consequence of TBM mixing as given in Eq. (3) is that it implies $\sin^2\theta_{12} = 1/3$, $\sin^2\theta_{23} = 1/2$ and $\sin\theta_{13} = 0$. Now to explain the current experimental observation on θ_{13} we consider an operator of order $1/\Lambda^3$:

$$-\delta\mathcal{L}_\nu = y_3\frac{(\ell H\ell H)\phi\eta}{\Lambda^3}\,, \tag{6}$$

where we have introduced two other SM singlet flavon fields ϕ and η which carry equal and opposite charges under the $U(1)$ symmetry but transform as 1 and $1'$ under A_4 respectively. The $U(1)$ charge assignment to these two flavons also ensures that ϕ and η do not take part in $(m_\nu)_0$. Thus, after flavor and electroweak symmetry breaking this term contributes to the light neutrino mass matrix as follows:

$$\delta m_\nu = \begin{pmatrix} 0 & 0 & d \\ 0 & d & 0 \\ d & 0 & 0 \end{pmatrix}, \tag{7}$$

where $d = y_3(v^2/\Lambda)\epsilon^2$ with $\epsilon = \langle\phi\rangle/\Lambda \equiv \langle\eta\rangle/\Lambda$. This typical flavor structure of the additional contribution in the neutrino mass matrix follows from the involvement of η field, which transforms as $1'$ under A_4 [29, 20]. This δm_ν can indeed generate the $\theta_{13} \neq 0$ in the same line as in [20, 22, 23]. Note that the choice of Z_2 symmetry presented in Table 1 also forbids the contributions to neutrino mass matrix proportional to $1/\Lambda^3$ (involving terms like $\ell H\ell H\phi_S\phi_T, \ell H\ell H\xi\phi_T, \ell H\ell H\phi_S\phi_T^\dagger$ and $\ell H\ell H\xi\phi_T^\dagger$) and thus ensuring Eq. (7) is the only contribution responsible for breaking the TBM mixing.

2.2 Dark sector and its interaction with neutrino sector

The dark sector associated with the present construction consists of a vector-like $SU(2)_L$ doublet $\psi^T = (\psi^0, \psi^-)$ and a neutral singlet fermion χ^0 [16], which are odd under the Z_2 symmetry as has already been mentioned in Table 1. These fermions are charged under an additional $U(1)$ flavor symmetry, but neutral under the existing symmetry in the neutrino sector (say the non-abelian A_4 and additional discrete symmetries required). Note that all the SM fields and the additional flavons in the neutrino sector except ϕ are neutral under this additional $U(1)$ symmetry. Since ψ and χ^0 are vector-like fermions, they can have bare masses, M_ψ and M_χ, which are not protected by the SM symmetry. The effective Lagrangian, invariant

under the symmetries considered, describing the interaction between the dark and the SM sector is then given by:

$$\mathcal{L}_{\rm int} = \left(\frac{\phi}{\Lambda}\right)^n \overline{\psi}\widetilde{H}\chi^0, \tag{8}$$

where n is not fixed at this stage. The above term is allowed provided the $U(1)$ charge of ϕ^n is compensated by ψ and χ^0 *i.e.* $nx = q_1 - q_2$. We will fix it later from phenomenological point of view.

When ϕ acquires a vev, the $U(1)$ symmetry breaks down and an effective Yukawa interaction is generated between the SM and the DM sectors. After electroweak symmetry is broken, the DM emerges as an admixture of the neutral component of the vector-like fermions ψ, *i.e.* ψ^0, and χ^0. The Lagrangian describing the DM sector and the interaction as a whole reads as

$$-\mathcal{L}_{\rm Yuk} \supset M_\psi \overline{\psi}\psi + M_\chi \overline{\chi^0}\chi^0 + \left[Y\overline{\psi}\widetilde{H}\chi^0 + \text{h.c.}\right], \tag{9}$$

where the effective Yukawa connecting the dark sector to the SM Higgs reads as $Y = \epsilon^n = \left(\frac{\langle\phi\rangle}{\Lambda}\right)^n$. We have already argued in introduction about our construction of dark matter sector. The idea of introducing vector-like fermions in the dark sector is also motivated by the fact that we expect a replication of the SM Yukawa type interaction to be present in the dark sector as well. Here the ϕ field plays the role of the messenger field similar to the one considered in [24]. See also [25] for some earlier efforts to relate A_4 flavor symmetry to DM. Note that the vev of the ϕ field is also instrumental in producing the term d to the neutrino mass matrix along with the vev of η. Since the d-term is responsible for generation of nonzero θ_{13} (will be discussed in the next section) a connection between non-zero $\sin\theta_{13}$ and DM interaction becomes correlated in our set-up.

A discussion about other possible terms allowed by the symmetries considered would be pertinent here. Terms like $\overline{\psi}\psi H^\dagger H/\Lambda$ and $\overline{\chi^0}\chi^0 H^\dagger H/\Lambda$ are actually allowed in the present set-up. However it turns out that their role is less significant compared to the other terms present. The reason is the following: firstly they could contribute to bare mass terms of ψ and χ^0 fields. However these contribution being proportional to v^2/Λ are insignificant as compared to M_ψ and M_χ. Similar conclusion holds for the Yukawa term as well. Secondly, they could take part in the DM annihilation. However as we will see, there also they do not have significant contribution because of the Λ suppression.

3 Phenomenology of the neutrino sector

Combining Eqs. (2) and (7), we get the light neutrino mass matrix as $m_\nu = (m_\nu)_0 + \delta m_\nu$. We have already seen that $(m_\nu)_0$ can be diagonalized by U_{TB} alone. Hence including δm_ν, rotation by U_{TB} results into the following structure of neutrino mass matrix:

$$m'_\nu = U_{TB}^T m_\nu U_{TB}, \tag{10}$$

$$= \begin{pmatrix} a-b-d/2 & 0 & \sqrt{3}d/2 \\ 0 & a+d & 0 \\ \sqrt{3}d/2 & 0 & -a-b+d/2 \end{pmatrix}. \tag{11}$$

So an additional rotation (by the U_1 matrix given below) is required to diagonalize m_ν,

$$(U_{TB}U_1)^T m_\nu (U_{TB}U_1) = \text{diag}(m_1 e^{i\gamma_1}, m_2 e^{i\gamma_2}, m_3 e^{i\gamma_3}) \tag{12}$$

where

$$U_1 = \begin{pmatrix} \cos\theta_\nu & 0 & \sin\theta_\nu e^{-i\varphi} \\ 0 & 1 & 0 \\ -\sin\theta_\nu e^{i\varphi} & 0 & \cos\theta_\nu \end{pmatrix}. \tag{13}$$

Here $m_{i=1,2,3}$ are the real and positive eigenvalues and $\gamma_{i=1,2,3}$ are the phases associated to these mass eigenvalues. We can therefore extract the neutrino mixing matrix U_ν as,

$$U_\nu = U_{TB}U_1U_m = \begin{pmatrix} \sqrt{\frac{2}{3}}\cos\theta_\nu & \frac{1}{\sqrt{3}} & \sqrt{\frac{2}{3}}e^{-i\varphi}\sin\theta_\nu \\ -\frac{\cos\theta_\nu}{\sqrt{6}} + \frac{e^{i\varphi}\sin\theta_\nu}{\sqrt{2}} & \frac{1}{\sqrt{3}} & -\frac{\cos\theta_\nu}{\sqrt{2}} - \frac{e^{-i\varphi}\sin\theta_\nu}{\sqrt{6}} \\ -\frac{\cos\theta_\nu}{\sqrt{6}} - \frac{e^{i\varphi}\sin\theta_\nu}{\sqrt{2}} & \frac{1}{\sqrt{3}} & \frac{\cos\theta_\nu}{\sqrt{2}} - \frac{e^{-i\varphi}\sin\theta_\nu}{\sqrt{6}} \end{pmatrix} U_m \,, \tag{14}$$

where $U_m = \mathrm{diag}(1, e^{i\alpha_{21}/2}, e^{i\alpha_{31}/2})$ is the Majorana phase matrix with $\alpha_{21} = (\gamma_1 - \gamma_2)$ and $\alpha_{31} = (\gamma_1 - \gamma_3)$, one common phase being irrelevant. The angle θ_ν and phase φ associated in U_1 can now be linked with the parameters: a, b, d involved in m_ν through Eq. (11).

Note that the parameters: a, b and d are all in general complex quantities. We define the phases associated with a, b, d as ϕ_a, ϕ_b and ϕ_d respectively. Also for simplifying the analysis, we consider $|y_1| = |y_3| = y$ and $|y_2| = k$. With these, θ_ν and φ can be expressed in terms of the parameters involved in the effective light neutrino mass matrix m'_ν as:

$$\tan 2\theta_\nu = \frac{\sqrt{3}\epsilon\cos\phi_{db}}{(\epsilon\cos\phi_{db} - 2\cos\phi_{ab})\cos\varphi}, \tag{15}$$

$$\tan\varphi = \frac{y}{k}\frac{\sin(\phi_{db} - \phi_{ab})}{\cos\phi_{db}}. \tag{16}$$

where $\phi_{ab} = \phi_a - \phi_b$ and $\phi_{db} = \phi_d - \phi_b$. Then comparing the standard U_{PMNS} parametrization and neutrino mixing matrix $U_\nu (= U_{TBM}U_1U_m)$ we obtain

$$\sin\theta_{13} = \sqrt{\frac{2}{3}}\,|\sin\theta_\nu|\,, \quad \delta = \arg[(U_1)_{13}]. \tag{17}$$

From Eq. (15) and (16) it is clear that, $\sin\theta_\nu$ may take positive or negative value depending on the choices of ϵ and y/k. For $\sin\theta_\nu > 0$, we find $\delta = \varphi$ using $\delta = \arg[(U_1)_{13}]$. On the other hand for $\sin\theta_\nu < 0$; δ and φ are related by $\delta = \varphi \pm \pi$. Therefore in both these cases we obtain $\tan\varphi = \tan\delta$ and hence Eq. (16) leads to

$$\tan\delta = \frac{y}{k}\frac{\sin(\phi_{db} - \phi_{ab})}{\cos\phi_{db}}. \tag{18}$$

The other two mixing angles follow the standard correlation with θ_{13} in A_4 models [26, 27].

Using Eq. (12), the complex light neutrino mass eigenvalues are evaluated as

$$m^c_{1,3} = \left[-b \pm \sqrt{a^2 - ad + d^2}\right], \tag{19}$$

$$m^c_2 = (a + d). \tag{20}$$

Correspondingly the real and positive mass eigenvalues of light neutrinos are determined as

$$m_1 = \alpha\frac{y}{k}\left[\left(P - \frac{k}{y}\right)^2 + Q^2\right]^{1/2}, \tag{21}$$

$$m_2 = \alpha\frac{y}{k}\left[1 + \epsilon^2 + 2\epsilon\cos(\phi_{ab} - \phi_{db})\right]^{1/2}, \tag{22}$$

$$m_3 = \alpha\frac{y}{k}\left[\left(P + \frac{k}{y}\right)^2 + Q^2\right]^{1/2}, \tag{23}$$

where

$$\alpha = \frac{k}{\Lambda}v^2\epsilon, \quad P = \left[\frac{1}{2}(A + \sqrt{A^2 + B^2})\right]^{1/2} \text{and } Q = \left[\frac{1}{2}(-A + \sqrt{A^2 + B^2})\right]^{1/2}, \tag{24}$$

with

$$A = (\cos 2\phi_{ab} + \epsilon^2 \cos 2\phi_{db} - \epsilon \cos(\phi_{ab} + \phi_{db})), \quad (25)$$

$$B = (\sin 2\phi_{ab} + \epsilon^2 \sin 2\phi_{db} - \epsilon \sin(\phi_{ab} + \phi_{db})). \quad (26)$$

Also, phases (γ_i) associated with each mass eigenvalues can be expressed as

$$\gamma_1 = \phi_b + \tan^{-1}\left(\frac{Q}{P - \frac{k}{y}}\right), \quad (27)$$

$$\gamma_2 = \phi_b + \tan^{-1}\left(\frac{\sin\phi_{ab} + \epsilon \sin\phi_{db}}{\cos\phi_{ab} + \epsilon\cos\phi_{db}}\right), \quad (28)$$

$$\gamma_3 = \pi + \phi_b + \tan^{-1}\left(\frac{Q}{P + \frac{k}{y}}\right). \quad (29)$$

Using the above expressions of absolute neutrino masses, we define the ratio of solar to atmospheric mass-squared differences as r,

$$r = \frac{\Delta m^2_\odot}{|\Delta m^2_{atm}|}, \quad (30)$$

with $\Delta m^2_\odot \equiv \Delta m^2_{21} = m_2^2 - m_1^2$ and $|\Delta m^2_{atm}| \equiv |\Delta m^2_{31}| = |m_3^3 - m_1^2|$. Then it turns out that both r and θ_{13} depends on $\epsilon, y/k$ and the relative phases: ϕ_{ab}, ϕ_{db}. The Dirac CP phase δ is also a function of these parameters only. As values of r and θ_{13} are precisely known from neutrino oscillation data, it would be interesting to constrain the parameter space of $\epsilon, y/k$ and the relative phases which can be useful in predicting δ. However analysis with all these four parameters is difficult to perform. So, below we categorize few cases depending on some specific choices of relative phases. In doing the analysis, following [7], the best fit values of $\Delta m^2_\odot = 7.6 \times 10^{-5}$ eV^2 and $|\Delta m^2_{atm}| = 2.48 \times 10^{-3}$ eV^2 are used for our analysis. r and $\sin\theta_{13}$ are taken as 0.03 and 0.1530 (best fit value [7]) respectively.

3.1 Case A : $\phi_{ab} = \phi_{db} = 0$

Here we make the simplest choice for the phases, $\phi_{ab} = \phi_{db} = 0$. Then the Eq. (15) becomes function of ϵ alone [20] as:

$$\tan 2\theta_\nu = \frac{\sqrt{3}\epsilon}{\epsilon - 2}. \quad (31)$$

Hence $\sin\theta_{13}$ depends only on ϵ where following Eq. (18), the Dirac CP phase is zero or π. The ϵ dependence of $\sin\theta_{13}$ is represented in Fig. 1. The horizontal patch in Fig. 1 denotes the allowed 3σ range of $\sin\theta_{13}$ ($\equiv$ 0.1330-0.1715) [7] which is in turn restrict the range of ϵ parameter (between 0.328 and 0.4125) denoted by the vertical patch in the same figure. Note that the interaction strength of DM with the SM particles depends on $\epsilon^n \equiv Y$. Therefore we find that the size of $\sin\theta_{13}$ is intimately related with the Higgs portal coupling of DM. This is the most significant observation of this paper. With the above mentioned range of ϵ, obtained from Fig. 1, the two other mixing angles θ_{12} and θ_{23} are found to be within the 3σ range.

Expressions for the real and positive mass eigenvalues are obtained from Eq. (21-23) and can be written as

$$m_1 = \alpha\frac{y}{k}\left|\sqrt{1 - \epsilon + \epsilon^2} - k/y\right|, \quad (32)$$

$$m_2 = \alpha\frac{y}{k}\left[1 + \epsilon\right], \quad (33)$$

$$m_3 = \alpha\frac{y}{k}\left[\sqrt{1 - \epsilon + \epsilon^2} + k/y\right]. \quad (34)$$

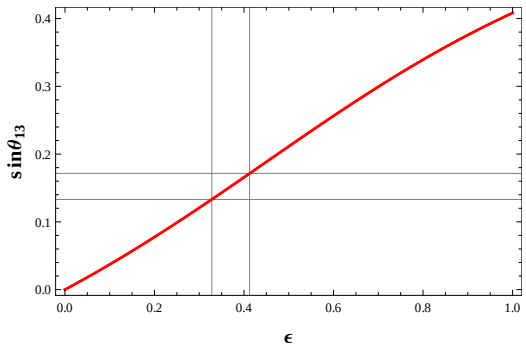

Figure 1: Plot of $\sin\theta_{13}$ against ϵ. 3σ range [7] of $\sin\theta_{13}$ (indicated by the horizontal lines) fixes ϵ in the range: 0.328-0.4125 (indicated by vertical lines).

With the above mass eigenvalues, one can write the ratio of solar to atmospheric mass-squared differences as defined in Eq. (30) as:

$$r = \frac{3\epsilon\frac{y}{k} - \frac{k}{y} + 2\sqrt{1-\epsilon+\epsilon^2}}{4\sqrt{1-\epsilon+\epsilon^2}}. \tag{35}$$

From Fig. 1, we have fixed ϵ range corresponding to 3σ range of $\sin\theta_{13}$. Now, to satisfy $r = 0.03$ [7], we vary the ratio of the coupling constants, y/k, against ϵ using Eq. (30) and (32-34). The result is presented in Fig. 2. The vertical patch there represents allowed region for ϵ fixed from Fig. 1 which determines the

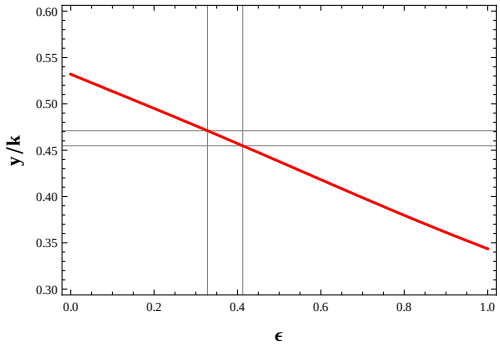

Figure 2: Contour plot of $r = 0.03$ in $y/k - \epsilon$ plane. The vertical lines represent the allowed range for ϵ (0.328-0.4125) corresponding to 3σ range of $\sin\theta_{13}$ which restricts the ratio y/k between 0.471 to 0.455 indicated by horizontal lines.

range of y/k to be within 0.471-0.455. After obtaining ϵ and the ratio y/k, we can now find the factor k/Λ (within α) in order to satisfy the solar mass-squared difference $\Delta m^2_\odot = m_2^2 - m_1^2 = 7.6\times10^{-5}$ eV^2 [7]. Using Eq. (32) and (33) we find this factor to be

$$\frac{k}{\Lambda} = \frac{1}{v^2\epsilon\frac{y}{k}}\sqrt{\frac{\Delta m^2_\odot}{\left[3\epsilon - \left(\frac{k}{y}\right)^2 + 2\frac{k}{y}\sqrt{1+\epsilon^2-\epsilon}\right]}}. \tag{36}$$

Considering the 3σ variation of $\sin\theta_{13}$, it falls within 1.97×10^{-15} GeV^{-1} to 1.60×10^{-15} GeV^{-1} with $v = 246$ GeV. Once we know about all parameters involved like $\epsilon, y/k, k/\Lambda$ with the specific choice of the phases (in this case $\phi_{ab} = \phi_{db} = 0$), it is straightforward to determine absolute neutrino masses and effective neutrino mass parameter involved in neutrinoless double beta decay using

$$|m_{ee}| = \left|m_1^2c_{12}^2c_{13}^2 + m_2^2s_{12}^2c_{13}^2e^{i\alpha_{21}} + m_3^2s_{13}^2e^{i(\alpha_{31}-2\delta)}\right| \tag{37}$$

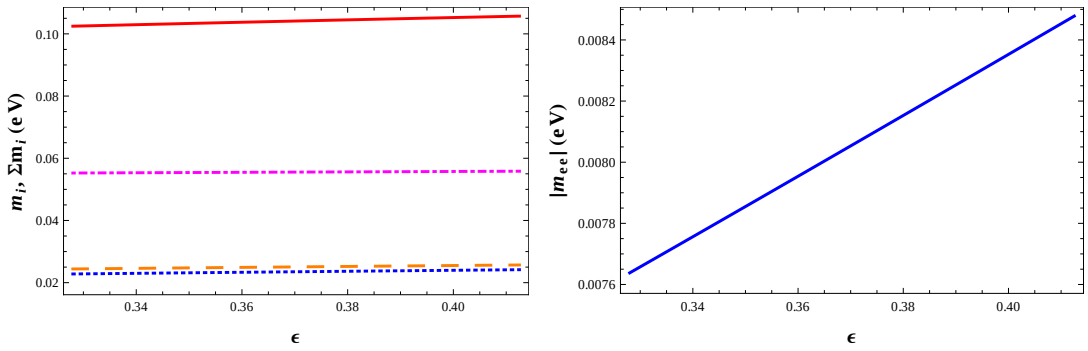

Figure 3: Left: Individual absolute neutrino masses (m_1- blue dotted line, m_2- orange dashed line, m_3- magenta dot-dashed line) and their sum (continuous red line) against ϵ (0.328-0.4125) corresponding to 3σ range of $\sin\theta_{13}$. Right: Effective neutrino mass parameter (continuous blues line) against ϵ (0.328-0.4125) corresponding to 3σ range of $\sin\theta_{13}$.

Parameters/Observable	Allowed Range
ϵ	0.328-0.4125
k/Λ (GeV^{-1})	1.97×10^{-15} - 1.60×10^{-15}
Σm_i (eV)	0.102 - 0.106
$\lvert m_{ee}\rvert$ (eV)	0.00764-0.00848

Table 2: Range of $\epsilon, k/\Lambda, \Sigma m_i, |m_{ee}|$ for 3σ range of $\sin\theta_{13}$ with $\phi_{ab} = \phi_{db} = 0$.

as shown in Fig. 3. We also have listed the summary of the predictions of these quantities in Table 2.

3.2 Case B : $\phi_{db} = 0$

Now we consider the case: $\phi_{db} = 0$. Then the relations for θ_ν and δ take the form

$$\tan 2\theta_\nu = \frac{\sqrt{3}\epsilon}{(\epsilon - 2\cos\phi_{ab})\cos\varphi}\,, \tag{38}$$

$$\tan\delta = -\frac{y}{k}\sin\phi_{ab}\,. \tag{39}$$

So from Eqs. (17, 38-39) and since $\tan\delta = \tan\varphi$, it is clear that unlike the Case A, here $\sin\theta_{13}$ depends not only on ϵ and y/k but also on the phase present in the theory, *i.e.* ϕ_{ab}. Therefore there would exist a one to one correspondence between ϵ and y/k in order to produce a specific value of $\sin\theta_{13}$ once a particular choice of δ has been made.

Now, with $\phi_{db} = 0$, absolute neutrino masses given in Eq. (21-23) are reduced to

$$m_1 = \alpha\frac{y}{k}\left[(P_1 - \frac{k}{y})^2 + Q_1^2\right]^{1/2}, \tag{40}$$

$$m_2 = \alpha\frac{y}{k}\left[1 + \epsilon^2 + 2\epsilon\cos\phi_{ab}\right]^{1/2}, \tag{41}$$

$$m_3 = \alpha\frac{y}{k}\left[(P_1 + \frac{k}{y})^2 + Q_1^2\right]^{1/2}, \tag{42}$$

with

$$P_1 = \left[\frac{1}{2}(A_1 + \sqrt{A_1^2 + B_1^2})\right]^{1/2},\ Q_1 = \left[\frac{1}{2}(-A_1 + \sqrt{A_1^2 + B_1^2})\right]^{1/2}, \tag{43}$$

$$A_1 = \left(\epsilon^2 + \cos 2\phi_{ab} - \epsilon\cos\phi_{ab}\right) \text{ and } B_1 = \left(\sin 2\phi_{ab} - \epsilon\sin\phi_{ab}\right). \tag{44}$$

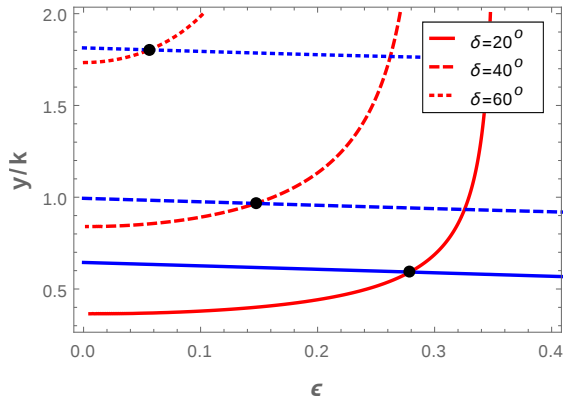

Figure 4: Contour plots for both $\sin\theta_{13} = 0.1530$ (shown in red continuous, dashed and dotted lines) and $r = 0.03$ (shown in blue continuous, dashed and dotted lines) for $\delta = 20°, \delta = 40°$ and $\delta = 60°$ respectively in ϵ-y/k plane. Black dots on each intersection represents solution for ϵ and y/k corresponding to each δ for $\phi_{db} = 0$.

The ratio of solar to atmospheric neutrino mass-squared differences takes the form

$$r = \frac{1}{4P_1\frac{k}{y}}\left[(1+\epsilon^2+2\epsilon\cos\phi_{ab}) - \left(P_1 - \frac{k}{y}\right)^2 - Q_1^2\right]. \tag{45}$$

Clearly, one finds that ϵ and y/k are the only parameters involved in both $\sin\theta_{13}$ and r once δ values are taken as input. Therefore, those values of ϵ and y/k are allowed which simultaneously satisfy data obtained for $\sin\theta_{13}$ and r from neutrino oscillation experiments. Here we have considered the best fit values from [7] and drawn contour plots for $\sin\theta_{13} = 0.1530$ and $r = 0.03$. Intersection of these contours then represents solutions for ϵ and y/k. Note that $\delta = 0$ case corresponds to the results obtained in Case A.

In Fig. 4, we have plotted typical contours obtained for $\sin\theta_{13} = 0.1530$ (red lines) and $r = 0.03$ (blue lines) for $\delta = 20°, \delta = 40°$ and $\delta = 60°$ respectively in ϵ-y/k plane. The intersecting points are denoted by black dots and represent the solution points for ϵ and y/k. In Table 3 we have listed estimations for ϵ and y/k for different δ values. Just like the previous case, after obtaining ϵ and y/k, we can find the factor k/Λ

δ	ϵ	y/k	k/Λ (10^{-15} GeV^{-1})	Σm_i (eV)	$\lvert m_{ee}\rvert$ (eV)
0°	0.372	0.463	1.756	0.1042	0.0222
10°	0.343	0.496	1.910	0.1068	0.0236
20°	0.279	0.592	2.361	0.1143	0.0274
30°	0.209	0.745	3.140	0.1267	0.0331
40°	0.147	0.966	4.405	0.1454	0.0409
50°	0.096	1.288	6.610	0.1743	0.0516
60°	0.056	1.803	11.10	0.2230	0.0682
61°	0.053	1.873	11.80	0.2298	0.0704
70°	0.026	2.798	23.22	0.3210	0.1002
80°	0.007	5.743	85.42	0.6173	0.1952

Table 3: Estimated values of various parameters and observables satisfying neutrino oscillation data for different values of δ with $\phi_{db} = 0$.

using the fact that it has to produce correct solar mass-squared difference $\Delta m^2_{\odot} = m_2^2 - m_1^2 = 7.6 \times 10^{-5}$ eV^2 [7]. For this, we employ Eq. (40) and (41). All these findings are mentioned in Table 3 including sum of the absolute masses (Σm_i) of all three light neutrinos and effective neutrino mass parameter involved in

neutrinoless double beta decay ($|m_{ee}|$) for different considerations of leptonic CP phase δ. In this analysis we observe that, for various values of δ between 0° to 360° there are certain points where same set of solutions for ϵ and y/k are repeated (*e.g.* solutions with δ is repeated for $|\pi - \delta|$). We should also employ the upper bound of sum of all three light neutrino masses ($\Sigma m_i < 0.23$ eV) coming from cosmological observation by Planck [14]. Once this is included, we note that some of the δ values need to be discarded as the corresponding sum of the masses exceeds 0.23 eV as seen from Table 3. We therefore conclude that the allowed values for δ are: between $0^\circ - 61^\circ$ (and also $119^\circ - 180^\circ$, $180^\circ - 241^\circ$ and $299^\circ - 360^\circ$).

3.3 Case C : $\phi_{ab} = 0$

When $\phi_{ab} = 0$, relations for θ_ν and δ take the form

$$\tan 2\theta_\nu = \frac{\sqrt{3}\epsilon \cos\phi_{db}}{(\epsilon\cos\phi_{db} - 2)\cos\varphi}, \tag{46}$$

$$\tan\delta = \frac{y}{k}\tan\phi_{ab}. \tag{47}$$

Here also $\sin\theta_{13}$ depends on $\epsilon, y/k$ and the phase involved ϕ_{db}. The real and positive mass eigenvalues can be written as

$$m_1 = \alpha\frac{y}{k}\left[(P_2 - \frac{k}{y})^2 + Q_2^2\right]^{1/2}, \tag{48}$$

$$m_2 = \alpha\frac{y}{k}\left[1 + \epsilon^2 + 2\epsilon\cos\phi_{db}\right]^{1/2}, \tag{49}$$

$$m_3 = \alpha\frac{y}{k}\left[(P_2 + \frac{k}{y})^2 + Q_2^2\right]^{1/2}, \tag{50}$$

with

$$P_2 = \left[\frac{1}{2}(A_2 + \sqrt{A_2^2 + B_2^2})\right]^{1/2},\ Q_2 = \left[\frac{1}{2}(-A_2 + \sqrt{A_2^2 + B_2^2})\right]^{1/2}, \tag{51}$$

where

$$A_2 = \left(1 + \epsilon^2\cos 2\phi_{db} - \epsilon\cos\phi_{db}\right) \text{ and } B_2 = \left(\epsilon^2\sin 2\phi_{db} - \epsilon\sin\phi_{db}\right). \tag{52}$$

The ratio of solar to atmospheric neutrino mass-squared differences takes the form

$$r = \frac{y/k}{4P_2}\left[(1 + \epsilon^2 + 2\epsilon\cos\phi_{db}) - (P_2 - k/y)^2 - Q_2^2\right]. \tag{53}$$

We then scan the parameter space for ϵ and y/k for various choices of δ so as to have $r = 0.03$ and $\sin\theta_{13} = 0.153$. In Fig. 5, we provide contour plots for $\sin\theta_{13} = 0.1530$ (red lines) and $r = 0.03$ (blue lines) for $\delta = 20^\circ, \delta = 40^\circ$ and $\delta = 60^\circ$. The intersection between $\sin\theta_{13}$ and r contours indicate the simultaneous satisfaction of them. Hence the intersections are indicated by black dots with which a pair of $\epsilon, y/k$ are attached. Similar to the previous two cases, here we estimate the k/Λ for each such pair of $\epsilon, y/k$ with a specific δ. This in turn provide an estimate of Σm_i and effective mass parameter $|m_{ee}|$ depending on the choice of δ. We provide these outcomes in Table 4.

3.4 Case D : $\phi_{ab} = \phi_{db} = \beta$

With $\phi_{ab} = \phi_{db} = \beta$, the mixing angle θ_ν turns out to be function of ϵ only and is given by

$$\tan 2\theta_\nu = \frac{\sqrt{3}\epsilon}{\epsilon - 2}, \tag{54}$$

while $\tan\delta$ becomes zero. Note that the expressions for the mixing angle θ_ν and δ are identical to the ones obtained in Case A. Therefore we use the constraint on ϵ obtained from Fig. 1 in order to satisfy 3σ allowed

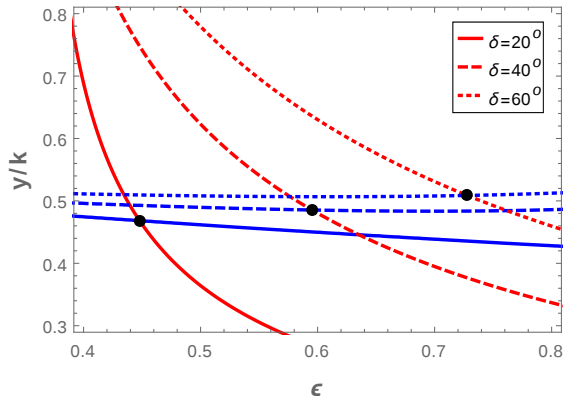

Figure 5: Contour plots for both $\sin\theta_{13} = 0.1530$ (shown in red continuous, dashed and dotted lines) and $r = 0.03$ (shown in blue continuous, dashed and dotted lines) for $\delta = 20°, \delta = 40°$ and $\delta = 60°$ respectively in ϵ-y/k plane. Black dots on each intersection represents solution for ϵ and y/k corresponding to each δ for $\phi_{ab} = 0$.

δ	ϵ	y/k	k/Λ (10^{-15} GeV^{-1})	Σm_i (eV)	$\lvert m_{ee}\rvert$ (eV)
0°	0.372	0.463	1.756	0.1042	0.0222
10°	0.393	0.464	1.670	0.1048	0.0225
20°	0.448	0.468	1.480	0.1065	0.0233
30°	0.520	0.475	1.300	0.1093	0.0245
40°	0.595	0.485	1.167	0.1128	0.0260
50°	0.666	0.497	1.065	0.1162	0.0273
60°	0.728	0.509	0.981	0.1182	0.0280
70°	0.782	0.519	0.901	0.1179	0.0275
80°	0.827	0.526	0.826	0.1152	0.0259

Table 4: Estimated values of various parameters and observables satisfying neutrino oscillation data for different values of δ with $\phi_{ab} = 0$.

range of $\sin\theta_{13}$. However the expressions for real and positive mass eigenvalues involve the common phase β and can be written as (following Eqs. (21-23))

$$m_1 = \alpha\frac{y}{k}\left[\left(\sqrt{1-\epsilon+\epsilon^2}\cos\beta - \frac{k}{y}\right)^2 + \left(\sqrt{1-\epsilon+\epsilon^2}\sin\beta\right)^2\right]^{1/2}, \tag{55}$$

$$m_2 = \alpha\frac{y}{k}\left[1+\epsilon\right], \tag{56}$$

$$m_3 = \alpha\frac{y}{k}\left[\left(\sqrt{1-\epsilon+\epsilon^2}\cos\beta + \frac{k}{y}\right)^2 + \left(\sqrt{1-\epsilon+\epsilon^2}\sin\beta\right)^2\right]^{1/2}. \tag{57}$$

Then following our approach for finding the range of parameters which would satisfy the oscillation parameters obtained from experimental data, we define the ratio of solar to atmospheric mass-squared differences as defined in Eq. (30) as

$$r = \frac{3\epsilon\frac{y}{k} - \frac{k}{y} + 2\cos\beta\sqrt{1-\epsilon+\epsilon^2}}{4|\cos\beta|\sqrt{1-\epsilon+\epsilon^2}}. \tag{58}$$

From Fig. 1 we fix $\epsilon = 0.372$ which would produce the best fit value of $\sin\theta_{13}$. Then, using the ratio of solar to atmospheric mass squared difference as given in Eq. (58), we can constrain y/k and $\cos\beta$. Here we

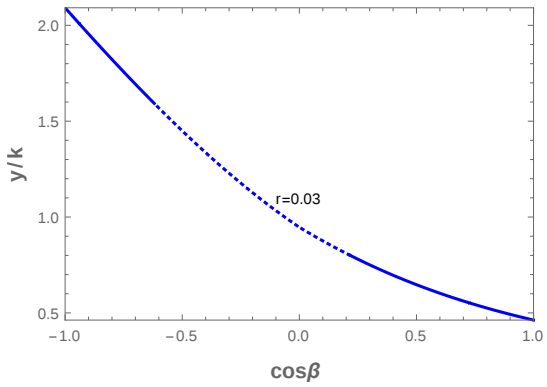

Figure 6: Contour plot for $r = 0.03$ in the $y/k - \cos\beta$ plane for $\phi_{db} = \phi_{ab} = \beta$. The disallowed range of $y/k, \cos\beta$ is indicated by the dotted portion.

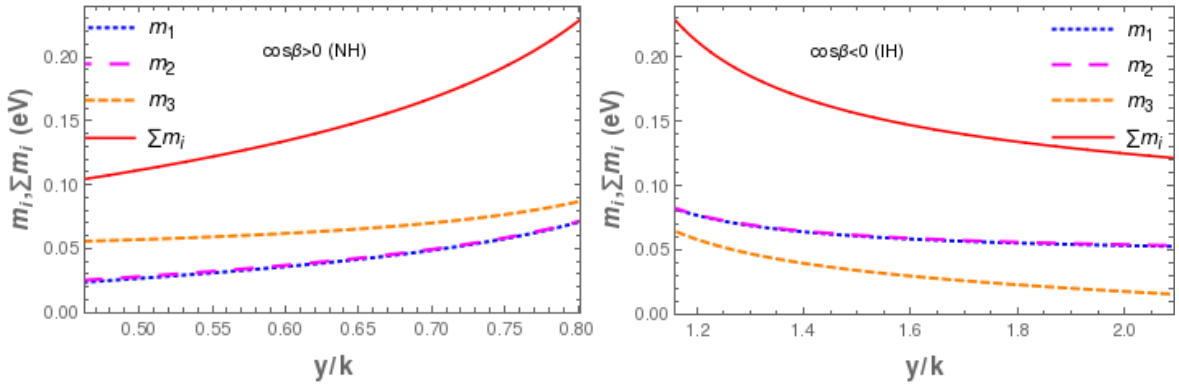

Figure 7: Absolute neutrino masses vs y/k (blue dotted, magenta large-dashed, orange dashed and red continuous lines represent m_1, m_2, m_3 and $\sum m_i$ respectively). The left panel is for $\cos\beta > 0$ and right panel is for $\cos\beta < 0$.

plot $r = 0.03$ contour in the y/k-$\cos\beta$ plane as shown in Fig. 6. For $-1 \leq \cos\beta \leq 1$. We observe that y/k falls within the range: $0.463 \leq\ y/k \leq 2.091$. Thus Fig. 6 establishes a correlation between y/k and $\cos\beta$. Now to find absolute neutrino masses we need to obtain k/Λ first. We can find k/Λ from the best fit value for solar mass squared difference, $m_2^2 - m_1^2 = 7.6 \times 10^{-5}$ eV^2, and is given by

$$\left(\frac{k}{\Lambda}\right)^2 = \frac{\Delta m_\odot^2}{4r(v^2\epsilon)^2 y/k|\cos\beta|\sqrt{1+\epsilon^2}-\epsilon}. \tag{59}$$

We have used Eq. (55-57) to obtain the above equation. Once ϵ is fixed at 0.372 and following Fig. 6 we know y/k and corresponding $\cos\beta$ (to have $r = 0.03$), we can use Eq. (59) to have an estimate for k/Λ. Now by knowing k/Λ, we have plotted absolute masses for light neutrinos in Fig. 7 by using Eq. (55-57). Here the left (right) panel is for $\cos\beta > 0 (< 0)$ and indicates normal (inverted) hierarchy for light neutrino masses. In Fig. 7, absolute neutrino masses m_1, m_2, m_3 and $\sum m_i$ are denoted by blue dotted, magenta large-dashed, orange dashed and red continuous lines respectively. Note that here we have plotted sum of the three absolute light neutrino masses consistent with the recent observation made by PLANCK, *i.e.* $\sum m_i \leq 0.23$ eV [38]. If we impose this constraint on the sum of absolute masses of the three light neutrinos, then the allowed region for y/k gets further constrained. The dotted portion in Fig. 6 represents this excluded part. Therefore the allowed region for y/k then turns out to be $0.463 \leqslant y/k \leqslant 0.802$ for $\cos\beta > 0$ (normal hierarchy) and $1.159 \leqslant y/k \leqslant 2.091$ for $\cos\beta < 0$ (inverted hierarchy). Finally in this case, the prediction for $|m_{ee}|$ found to be within $0.022\,\text{eV} < |m_{ee}| < 0.039\,\text{eV}$ for normal hierarchy and

$0.016\,\text{eV} < |m_{ee}| < 0.035\,\text{eV}$ for inverted hierarchy.

4 Phenomenology of DM Sector

The dark sector consists of two vector-like fermions: a fermion doublet ψ and a singlet χ. The corresponding Lagrangian respecting the $U(1)$ and other discrete symmetries is provided in Eq. (9). At this stage we can remind ourselves about the minimality of the construction in terms of choice of constituents of the dark sector. Note that a vector-like singlet fermion alone can not have a coupling with the SM sector at the renormalizable level and thereby its relic density is expected to be over abundant (originated from interaction suppressed by the new physics scale Λ). On the contrary, a vector-like fermion doublet alone can have significant annihilation cross section from its gauge interaction with the SM sector and thereby we would expect the corresponding dark matter relic density to be under-abundant. Hence we can naturally ask the question whether involvement of a singlet and a doublet vector-like fermions can lead to the dark matter relic density at an acceptable level. It then crucially depends on the mixing term between the singlet and the doublet fermions, *i.e.* on $m_D = Yv$. We expect a rich phenomenology out of it particularly because the coupling Y depends on the parameter ϵ through $Y = \epsilon^n$ where ϵ plays an important role in the neutrino physics as evident from our discussion in the previous section. We aim to restrict n phenomenologically.

The electroweak phase transition along with the $U(1)$ breaking give rise to the following mass matrix in the basis (χ^0, ψ^0)

$$\mathcal{M} = \begin{pmatrix} M_\chi & m_D \\ m_D & M_\psi \end{pmatrix}. \tag{60}$$

We obtain mass eigenstates ψ_1 and ψ_2 with masses M_1 and M_2 respectively after diagonalization of the above matrix as

$$\begin{aligned} \psi_1 &= \cos\theta_d \chi^0 + \sin\theta_d \psi^0, \\ \psi_2 &= \cos\theta_d \psi^0 - \sin\theta_d \chi^0, \end{aligned} \tag{61}$$

where $\tan\theta_d = 2m_D/(M_\psi - M_\chi)$. We will work in the regime where $m_D << M_\psi, M_\chi$. This choice would be argued soon. However this is not unnatural as the dark matter is expected to interact weakly. In this limit, the mass eigenvalues are found to be

$$\begin{aligned} M_1 &\approx M_\chi - \frac{m_D^2}{M_\psi - M_\chi}, \\ M_2 &\approx M_\psi + \frac{m_D^2}{M_\psi - M_\chi}. \end{aligned} \tag{62}$$

In this small mixing limit, we can write $M_\psi - M_\chi \simeq M_2 - M_1 = \Delta M$. Therefore the mixing angle θ_d can be approximately represented by

$$\sin 2\theta_d \simeq \frac{2Yv}{\Delta M}. \tag{63}$$

Then as evident from Eqs. (61), ψ_1 is dominantly the singlet having a small admixture with the doublet. We assume it to be the lightest between the two (*i.e.* $M_1 < M_2$) and forms the DM component of the universe. In the physical spectrum, we also have a charged fermion $\psi^+(\psi^-)$ with mass $M^+(M^-) = M_1 \sin^2\theta_d + M_2 \cos^2\theta_d$, in the limit $\theta_d \to 0$, $M^\pm = M_2 = M_\psi$. In this section, we will discuss the relic density of dark matter as a function of Y. Although Y represents Yukawa coupling of the DM with SM Higgs, in presence of a singlet and doublet fermions, Y is also a function of the mixing angle $\sin\theta_d$ as well as the mass splitting (ΔM) which crucially controls DM phenomenology as we demonstrate in the following discussion.

Note that ψ_0 being the gauge doublet, it carries the gauge interactions and hence, the physical mass eigenstates including the DM have the following interaction with Z, W bosons as :

$$\frac{g}{\sqrt{2}}\overline{\psi_0}\gamma^\mu W_\mu^+ \psi^- + \text{h.c.} \to \frac{g\sin\theta_d}{\sqrt{2}}\overline{\psi_1}\gamma^\mu W_\mu^+ \psi^- + \frac{g\cos\theta_d}{\sqrt{2}}\overline{\psi_2}\gamma^\mu W_\mu^+ \psi^- + \text{h.c.}\,, \tag{64}$$

$$\frac{g}{2\cos\theta_w}\overline{\psi_0}\gamma^\mu Z_\mu\psi_0 \to \frac{g}{2\cos\theta_w}\left(\sin^2\theta_d\overline{\psi_1}\gamma^\mu Z_\mu\psi_1 + \sin\theta_d\cos\theta_d(\overline{\psi_1}\gamma^\mu Z_\mu\psi_2 + \overline{\psi_2}\gamma^\mu Z_\mu\psi_1) + \cos^2\theta_d\overline{\psi_2}\gamma^\mu Z_\mu\psi_2\right) . \tag{65}$$

The relic density of the dark matter (ψ_1) is mainly dictated by annihilations through (i) $\overline{\psi_1}\psi_1 \to W^+W^-, ZZ$ through $SU(2)_L$ gauge coupling and (ii) $\overline{\psi_1}\psi_1 \to hh$ through Yukawa coupling introduced in Eq. 8. The relevant processes are indicated in Fig. 8. The other possible channels are mainly co-annihilation of ψ_1 with ψ_2 (see Fig. 9) and $\psi^\pm$ (see Fig. 10) which would dominantly contribute to relic density in a large region of parameter space [16, 28, 31, 32, 33] as can be seen once we proceed further. At this stage we can argue on our choice of making θ_d small, or in other word why the mixing with doublet is necessary to be small for the model to provide a DM with viable relic density. This is because the larger is the doublet content in DM ψ_1, the annihilation goes up significantly in particular through $\psi_1\overline{\psi_1} \to W^+W^-$ through Z and hence yielding a very small relic density. So in this limit, ψ_2 is dominantly a doublet having a small admixture with the singlet one. This implies that ψ_2 mass is required to be larger than 45 GeV in order not to be in conflict with the invisible Z-boson decay width.

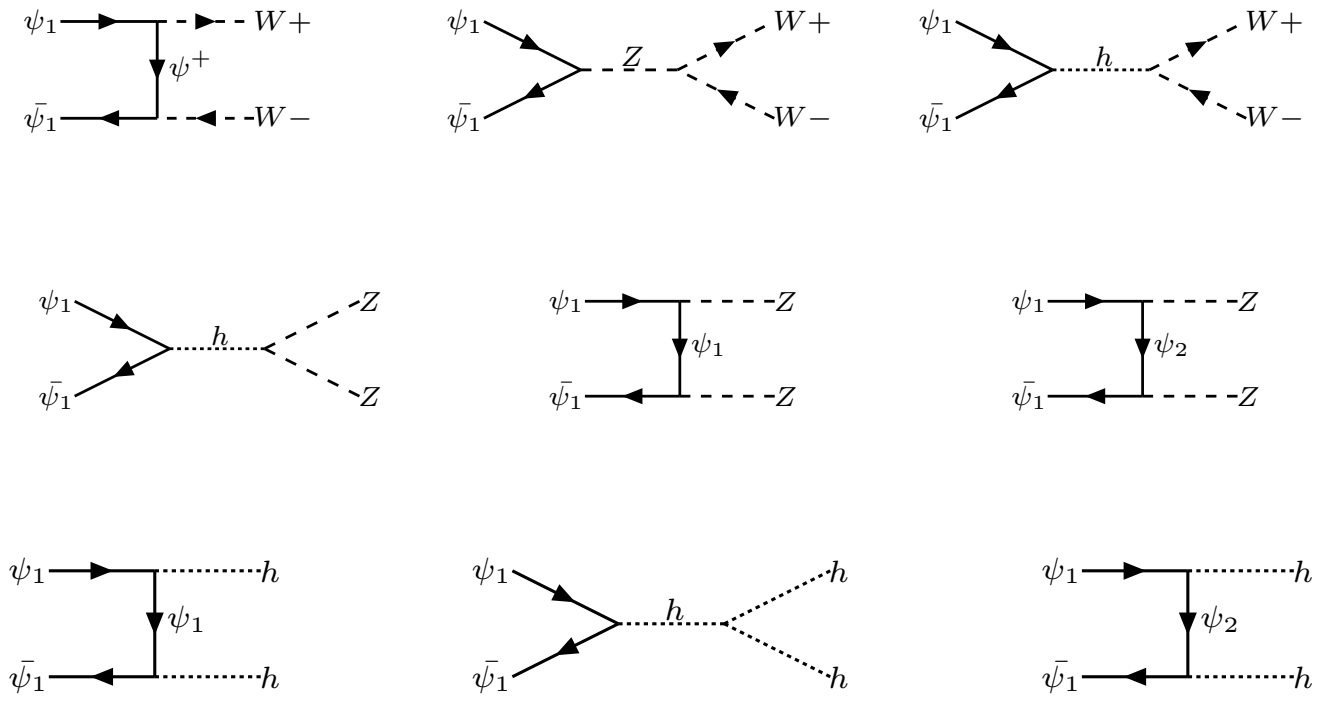

Figure 8: Dominant Annihilation processes to Higgs and Gauge boson final states.

The relic density of the ψ_1 DM with mass M_1 can be given by [28]

$$\Omega_{\psi_1}h^2 = \frac{1.09\times10^9\ \text{GeV}^{-1}}{g_\star^{1/2}M_{PL}}\frac{1}{J(x_f)}\,, \tag{66}$$

where $J(x_f)$ is given by

$$J(x_f) = \int_{x_f}^{\infty}\frac{\langle\sigma|v|\rangle_{eff}}{x^2}\ dx\,. \tag{67}$$

Here $\langle\sigma|v|\rangle_{eff}$ is the thermal average of dark matter annihilation cross sections including contributions from

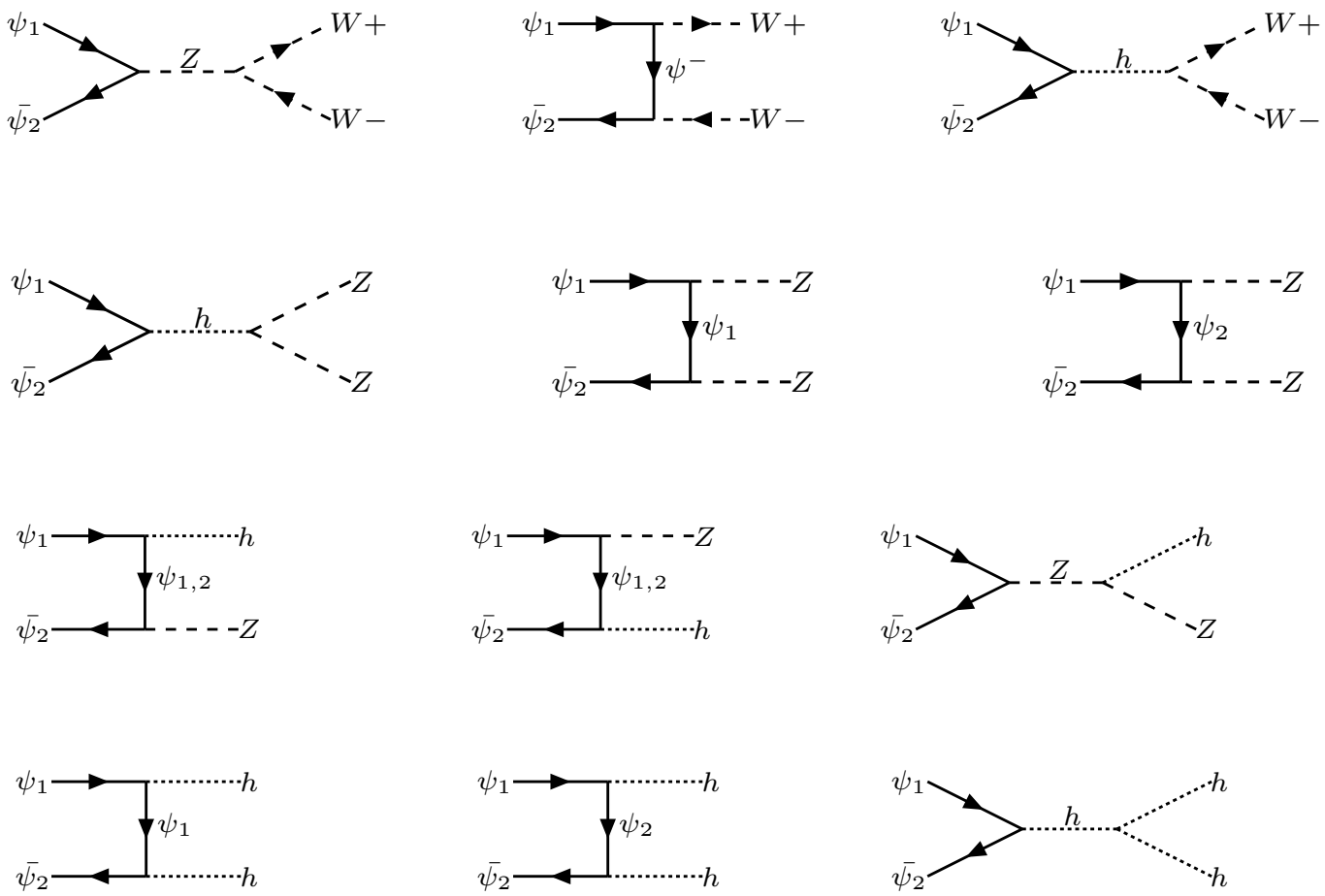

Figure 9: Dominant Co-Annihilations $\psi_1\bar{\psi}_2 \to SM$ to Higgs and Gauge boson final states.

co-annihilations as follows:

$$\begin{aligned}\langle\sigma|v|\rangle_{eff} =& \frac{g_1^2}{g_{eff}^2}\sigma(\overline{\psi_1}\psi_1) + 2\frac{g_1 g_2}{g_{eff}^2}\sigma(\overline{\psi_1}\psi_2)(1+\Delta)^{3/2}exp(-x\Delta) \\ &+ 2\frac{g_1 g_3}{g_{eff}^2}\sigma(\overline{\psi_1}\psi^-)(1+\Delta)^{3/2}exp(-x\Delta) \\ &+ 2\frac{g_2 g_3}{g_{eff}^2}\sigma(\overline{\psi_2}\psi^-)(1+\Delta)^{3}exp(-2x\Delta) + \frac{g_2 g_2}{g_{eff}^2}\sigma(\overline{\psi_2}\psi_2)(1+\Delta)^{3}exp(-2x\Delta) \\ &+ \frac{g_3 g_3}{g_{eff}^2}\sigma(\psi^+\psi^-)(1+\Delta)^{3}exp(-2x\Delta)\,.\end{aligned} \tag{68}$$

In the above equation g_1,g_2 and g_3 are the spin degrees of freedom for ψ_1, ψ_2 and ψ^- respectively. Since these are spin half particles, all g's are 2. The freeze-out of ψ_1 is parameterised by $x_f = \frac{M_1}{T_f}$, where T_f is the freeze out temperature. Δ depicts the mass splitting ratio as $\Delta = \frac{M_2 - M_1}{M_1} = \frac{\Delta M}{M_1}$, where M_2 stands for the mass of both ψ_2 and $\psi^{\pm}$. The effective degrees of freedom g_{eff} in Eq. (68) is given by

$$g_{eff} = g1 + g_2(1+\Delta)^{3/2}exp(-x\Delta) + g_3(1+\Delta)^{3/2}exp(-x\Delta)\,. \tag{69}$$

As it turns out from the above discussion, the dark-sector phenomenology in our set-up is mainly dictated by three parameters $\sin\theta_d, M_1$ and ΔM. However we will keep on changing $\sin\theta_d$ and/or ΔM dependence

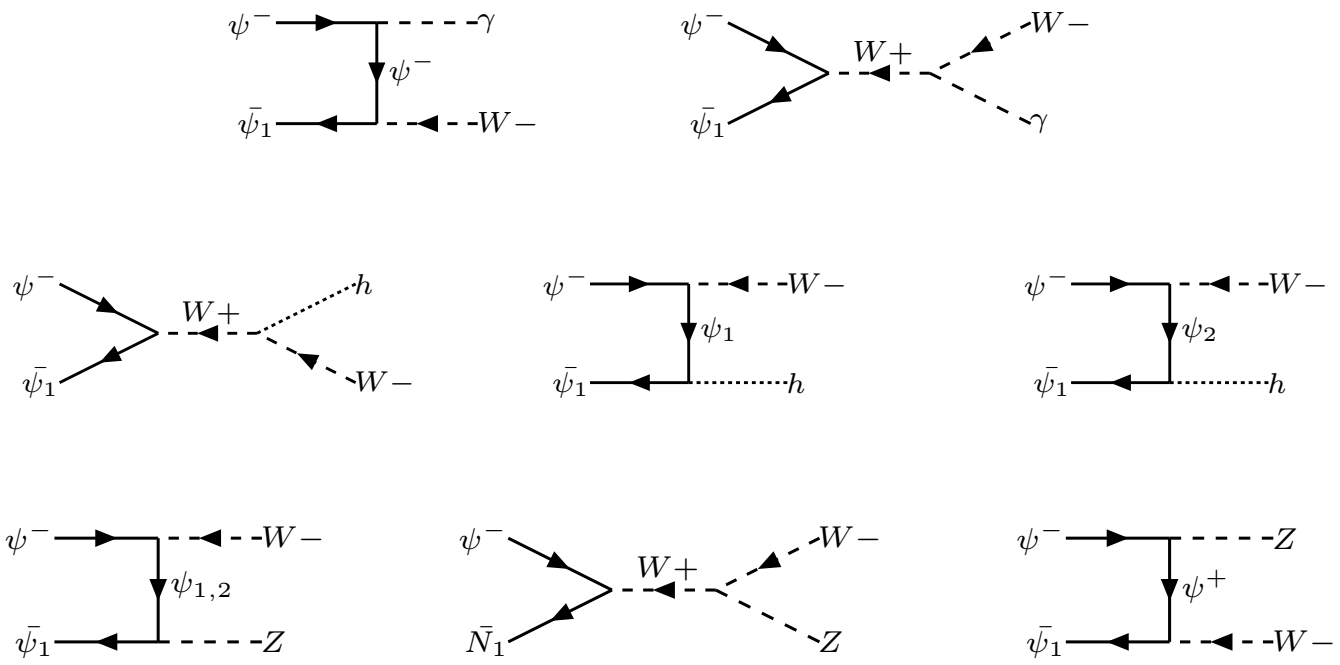

Figure 10: Dominant Co-Annihilation $\bar{\psi}_1\psi^- \to SM$ to Higgs and Gauge boson final states.

with Y wherever required using Eq.(63). In the following we use the code `MicrOmegas` [34] to find the allowed region of correct relic abundance for our DM candidate ψ_1 satisfying WMAP [13] constraint [5]

$$0.094 \leq \Omega_{\rm DM}h^2 \leq 0.130\,. \tag{70}$$

In Fig. 11 we plot relic density versus DM mass M_1 for different choices of $\sin\theta_d = 0.1, 0.2$ and 0.3 (represented by blue, green and orange dotted lines respectively) while keeping the mass difference ΔM fixed at 50 GeV in the left panel and at $\Delta M = 400$ GeV in the right panel. The choice of various $\sin\theta_d$ can be translated into different values of Y as well, through Eq. (63) since ΔM is kept fixed. Then it is equivalent to say that the blue, green and orange dotted lines in the left panel ($\Delta M = 50$ GeV) represent $Y=$ 0.02, 0.04, 0.058 respectively. In a similar way, the blue, green and orange dotted lines in the right panel ($\Delta M = 400$ GeV) are for $Y = 0.16, 0.32, 0.46$ respectively. We infer that as the mixing increases or in other words Y increases (ΔM is fixed), the doublet component starts to dominate (see Eq. (63)) and hence give larger cross-section which leads to a smaller DM abundance for a particular M_1. Note that $\sin\theta_d = 0.3$ ($Y = 0.058$ (0.46) with $\Delta M = 50$ (400) GeV) can barely satisfy relic density, where annihilations through Z mediation becomes large. Another interesting point to note comparing the left and right side of Fig. 11 is the effect of ΔM. If we compare blue lines in both of the figures (at a particular M_1 value say), they correspond to different $Y = \{0.02, 0.16\}$ and different sets of $(Y, \Delta M)$ as = (0.058, 50 GeV) for left and (0.16, 400 GeV) for right panel. Larger Y gives larger annihilations through Higgs Yukawa however we see that relic density in the right hand side is more than in the left, in particular for M_1 400 GeV. This is precisely because a large contribution to the relic density comes from the co-annihilation channels as $\overline{\psi_2}\psi_1 \to SM$ or $\overline{\psi^+}\psi_1 \to SM$. This co-annihilation contribution is very small for larger ΔM (400 GeV for example), however gives a significant contribution for lower $\Delta M = 50$ GeV (depending on DM mass though) in the left hand side of Fig. 11 yielding a larger effective annihilation cross-section with co-annihilation.

[5] The range we use corresponds to the WMAP results; the PLANCK constraints $0.112 \leq \Omega_{\rm DM}h^2 \leq 0.128$ [14], though more stringent, do not lead to significant changes in the allowed regions of parameter space.

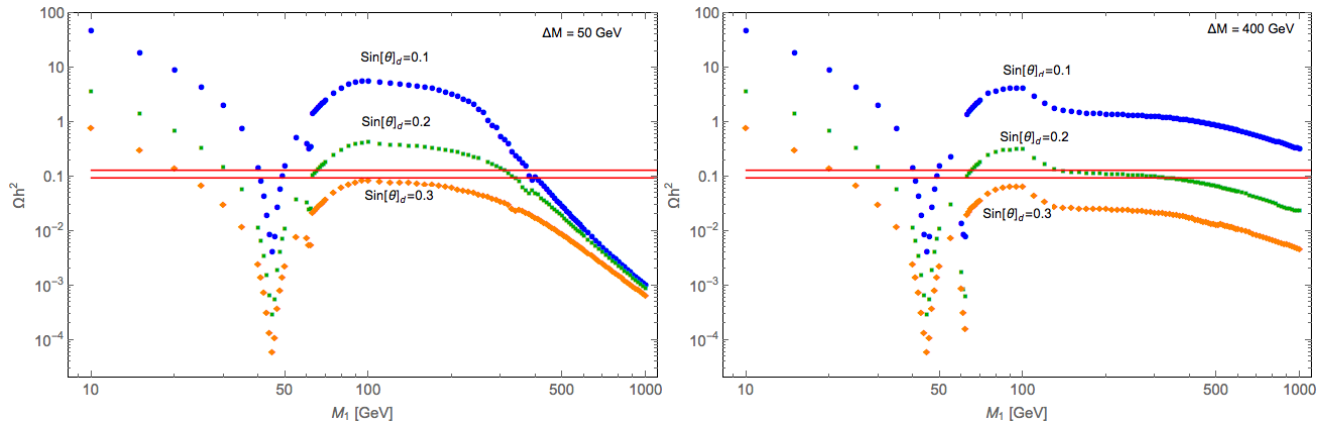

Figure 11: Relic density vs DM mass M_1 (in GeV) for different choices of $\sin\theta_d = \{0.1, 0.2, 0.3\}$ with $\Delta M = 50$ GeV [left] (corresponding to $Y = \{0.02, 0.04, 0.058\}$ with blue, green, orange respectively) and $\Delta M = 400$ GeV [right] (corresponding to $Y = \{0.16, 0.32, 0.46\}$ with Blue, Green, Orange respectively). Horizontal lines define the correct relic density.

We also clearly note the Z resonance at $M_1 = M_Z/2 \sim 45$ GeV and a Higgs resonance at $M_1 = M_H/2 \sim 63$ GeV. We can also note that with larger ΔM, which is larger Y (in the right hand side), the Higgs resonance is more prominent for obvious reasons.

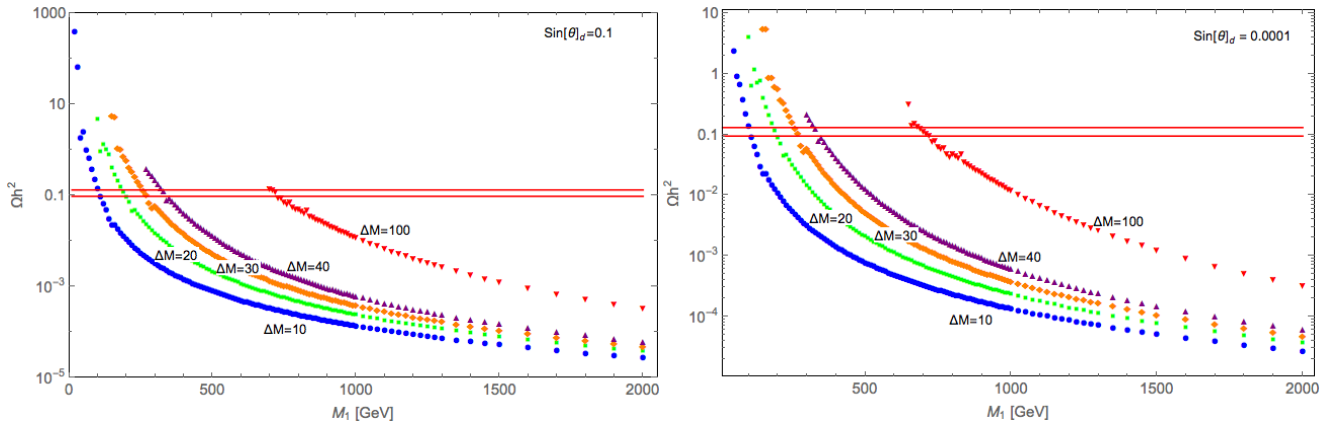

Figure 12: Left: Ωh^2 versus Dark matter mass M_1 (in GeV) for $\sin\theta_d = 0.1$ and $\Delta M = \{10, 20, 30, 40, 100\}$ (blue, green, orange, purple, red respectively). Right: Same as left but in terms of $\sin\theta_d = 0.0001$. Horizontal lines indicate correct relic density.

In order to show the effect of co-annihilations more closely, we draw Fig. 12. One can see the ΔM dependency on relic density for a specific choice of mixing angle. In the left panel we choose $\sin\theta_d = 0.1$ and that in the right panel for $\sin\theta_d = 0.0001$. The slices with constant ΔM is shown for $\Delta M = \{10, 20, 30, 40, 100\}$ GeV in blue, green, orange, purple, red lines respectively. We note here, that with larger ΔM, the annihilation cross-section increases due to enhancement in Yukawa coupling ($Y \propto \Delta M$ as $\sin\theta_d$ is fixed). However, co-annihilation decreases due to increase in ΔM as $\sigma \propto e^{-\Delta M}$. As co-annihilation dominates in this region of parameter space, the decrease in co-annihilation cross-section is much more than the increase in the annihilation channels, eventually leading to a larger relic density with increasing ΔM for a given value M_1. Hence the bigger is the ΔM, the larger is the DM mass required to satisfy relic density

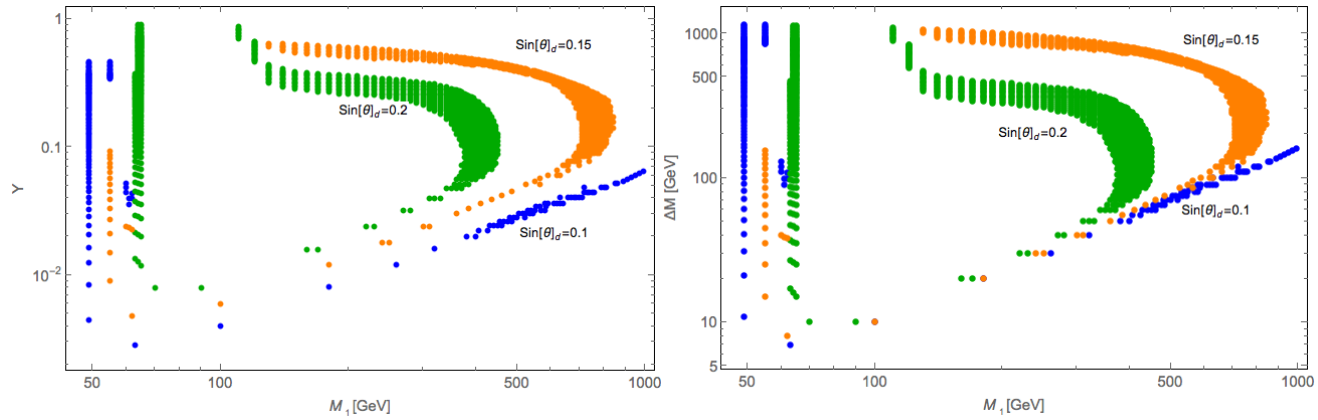

Figure 13: Left: Y versus M_1 (in GeV) for correct relic density (Eq. 70). $\sin\theta_d = 0.1,\ 0.2,\ 0.15$ (blue, green and orange respectively) has been chosen, while ΔM vary arbitrarily. Right: Same plot in $M_1 - \Delta M$ plane.

with mixing angle $\sin\theta_d \leq 0.1$.

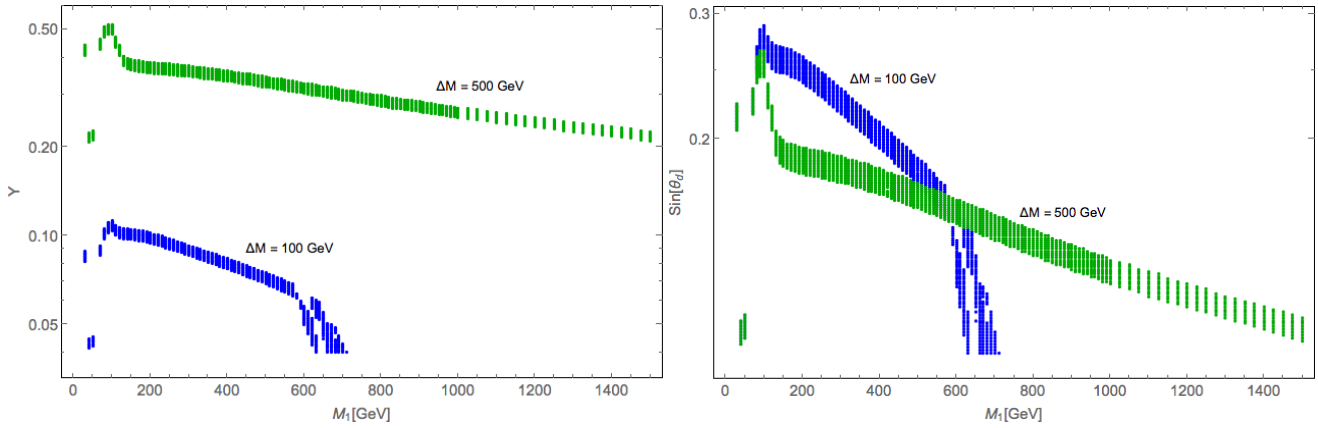

Figure 14: Left: Y versus M_1 (in GeV) for correct relic density (Eq. 70) with fixed $\Delta M = 100,\ 500$ GeV (blue and green respectively) has been chosen, while $\sin\theta_d$ vary. Right: Same plot in $M_1 - \sin\theta_d$ plane.

In Fig. 13 (left), we plot Y versus M_1 to produce correct relic density with $\sin\theta_d = \{0.1,\ 0.15,\ 0.2\}$ (blue, orange, green respectively). In order to be consistent with Eq.(63), ΔM has to be adjusted accordingly. It points out a relatively wide DM mass range satisfy the relic density constraint. It also shows that for $\sin\theta_d = 0.1$ (generally true for $\sin\theta_d \leq 0.1$), the annihilations are never enough to produce correct density and co-annihilations play a crucial part resulting the blue curve rising with the DM mass. For $\sin\theta_d = 0.2$ (green patch), smaller DM mass regions get contributions from co-annihilation with small Y and annihilations only for large Y, while the region close to DM mass 400 GeV has a significant contribution from Z mediation. In Fig. 13 (right), we show regions of correct density in $M_1 - \Delta M$ plane for same choices of $\sin\theta_d = \{0.1,\ 0.15,\ 0.2\}$ (blue, orange, green respectively).

However, there is another way of showing $Y - M_1$ dependence by keeping ΔM fixed while adjusting the mixing angle $\sin\theta_d$ appropriately. This is shown in the left panel of Fig. 14. Two cases have been presented: $\Delta M = 100$ GeV (in blue) and $\Delta M = 500$ GeV (green). This is clearly understood that with larger ΔM, a larger Y is favored for a specific DM mass in order to satisfy the correct relic abundance. With $\Delta M =$

100 GeV we also note that Y drops substantially around $M_1 \sim 600$ GeV. This is because around this value, co-annihilation process starts contributing and hence it requires a further drop in Y (in terms of mixing angle θ_d) to obtain right relic density. In the right side of Fig. 14, we show correct relic density region in terms of $M_1 - \sin\theta_d$, for fixed $\Delta M = 100$ GeV (blue), 500 GeV (green). Here also, we see that for $\Delta M = 100$ GeV, $\sin\theta_d$ drops around $M_1 \simeq 600$ GeV as co-annihilation starts contributing there. For $\Delta M = 600$ GeV, this phenomena occurs at a very large DM mass and can't be seen in the plot. Resonance drops both in $Y - M_1$ and $\sin\theta_d - M_1$ plots can be observed for $M_1 \sim M_H/2$ and $M_1 \sim M_Z/2$.

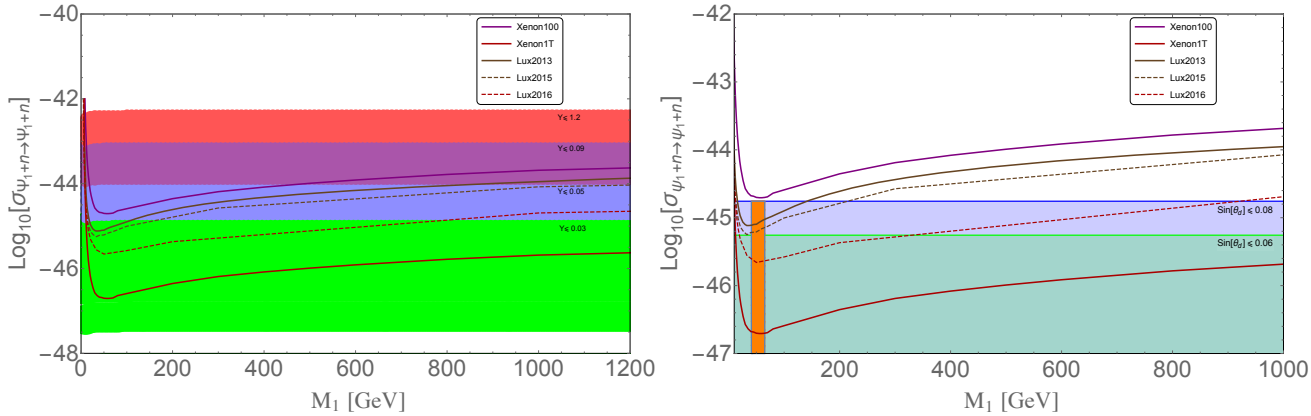

Figure 15: Spin independent direct search cross-section as a function of DM mass. Left: Different Y ranges are indicated $Y : \{0.001 - 0.03\}$ (green), $Y : \{0.03 - 0.05\}$ (blue), $Y : \{0.05 - 0.09\}$ (purple) and $Y : \{0.09 - 0.12\}$ (red). $\Delta M = 100$ GeV is used for the scan; Right: Allowed ranges of $\sin\theta_d \leq 0.06, 0.08$ (green and blue regions respectively) are shown. The resonance region is separately indicated in orange. Constraints from Xenon100, Lux 2013, 2015, 2016 data and predictions of Xenon1T are presented.

The direct search of DM ψ_1 has two different channels of interactions, through Z and H mediation, where the one through Z mediation dominates over H mediated interaction because of $SU(2)$ gauge coupling. It turns out that the most stringent constraint on the model and hence on the portal coupling Y ($\simeq \sin 2\theta_d \Delta M/(2v)$) comes from the direct search of DM from updated LUX data [36] as demonstrated in Fig. 15. Restricting direct search cross-section to experimental limit actually puts a stringent bound on mixing angle $\sin\theta_d$ to tame Z-mediated diagram in particular. We see that the bound from LUX, constraints the coupling: $Y \sim 0.03$ for DM masses $\gtrsim 800$ GeV (green regions) in the LHS of Fig. 15. The Yukawa coupling needs to be even smaller for $M_1 \simeq 200$ GeV. Though large couplings are allowed by correct relic density, they are highly disfavored by the direct DM search at terrestrial experiments. Note that these direct search constraints are less dependent on ΔM as to the mixing angle, which plays otherwise a crucial role in the relic abundance of DM. This is simple to appreciate as co-annihilations affect relic density co-scattering doesn't affect direct search. In particular, the one portrayed in LHS of Fig. 15, has a constant $\Delta M = 100$ GeV. In the right side of Fig. 15, we show the parameter space satisfied by relic density constraint for $\sin\theta_d = 0.08, 0.06$ (blue and green regions respectively) to direct search constraints. The direct search tightly constraints the mixing angle to $\sin\theta_d \leq 0.08$, allowing DM masses as heavy as 900 GeV. Tighter constraint in mixing angle, for example, $\sin\theta_d \leq 0.06$, allows smaller DM mass ≥ 400 GeV as can be seen from the cross-over of LUX constraint with relic density allowed parameter space. It is important to note that given a constant $\sin\theta_d \leq 0.1$, the relic density allowed space of the model solely relies on co-annihilation, with $\Delta M \leq 100$ GeV. Hence, direct search cross-section is almost a straight line for a small and constant $\sin\theta_d$ in relic density allowed parameter space as seen in the RHS of Fig. 15. We also have indicated the resonance region in orange where the spin independent direct search cross-section is not linear to mixing angle for relic density allowed parameter space.

In summary, the dark sector phenomenology with the inclusion of vector-like fermions provides a simple

extension to SM, with a rich phenomenology with a large region of allowed parameter space from relic density constraints. Direct search on the other hand constrains the mixing to a small value ≤ 0.08, allowing co-annihilation to play a dominant part to keep the model alive. We will focus on the correlations to non-zero θ_{13} and DM in the following section with the results obtained from above analysis.

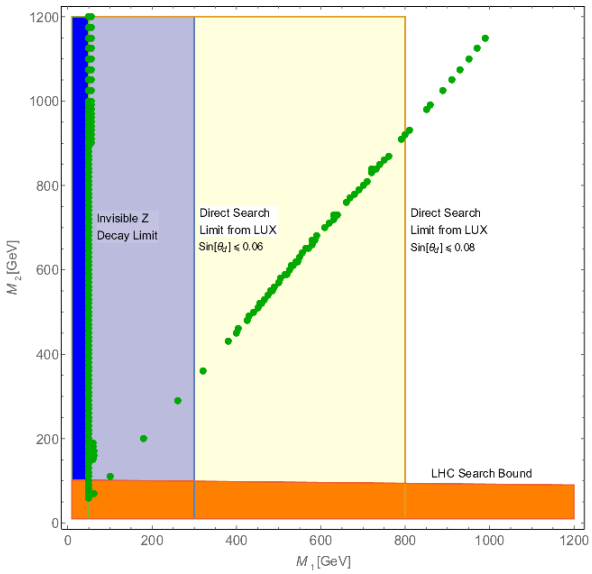

Figure 16: Summary of all constraints in $M_1 - M_2$ parameter space from relic density with $\sin\theta_d = 0.08$ (green dots), direct search (light orange region is forbidden by updated LUX with $\sin\theta_d \sim 0.08$ and lilac region is forbidden for $\sin\theta_d \sim 0.06$), invisible Z-decay (blue region is forbidden) and collider (LHC) search limit (orange region is disallowed).

We can now put together all the constraints for a specific choice of $\sin\theta_d = 0.08$ into the plane of $M_1 - M_2$ to show the allowed parameter space of the model. This is what we have done in Fig. 16 following

$$\begin{aligned}
\text{Inv Z decay} : \mathrm{M_1} < \frac{\mathrm{M_z}}{2} \sim 45\ \text{GeV} \rightarrow \sin\theta_d \lesssim 0.00125 \\
\text{Inv H decay} : \mathrm{M_1} < \frac{\mathrm{M_h}}{2} \sim 63\ \text{GeV} \rightarrow \sin\theta_d \lesssim 0.1 \\
\text{Relic Density} : \mathrm{M_2} \lesssim \mathrm{M_1} + 100\ \text{GeV for}\ \sin\theta_d \lesssim 0.1 \\
\text{Direct Search} : \mathrm{M_1} \geq 800(400)\ \text{GeV for}\ \sin\theta_d \sim 0.08(0.06) \\
\text{Collider Bound} : \mathrm{M_2} \simeq \mathrm{M^{\pm}} \geq 101\ \text{GeV for}\ \sin\theta_d \sim 0.08.
\end{aligned}$$

We choose $\sin\theta_d = 0.08$ as a reference value as it satisfies all of the constraints discussed here. We see that a sizable part of the DM parameter space is allowed shown by the green dotted points, excepting for the direct search bound shown by lilac band, a blue band disfavored by the Invisible Z decay and orange band disfavored by direct collider search data [37]. One should also note here that if we choose a smaller $\sin\theta_d$ to illustrate the case, a larger DM mass region is allowed by direct search constraint, for example lilac region shrinks to $M_1 \simeq 400$ GeV with $\sin\theta_d = 0.06$ while other constraints remain the same. Green dotted points show relic density allowed regions of the model in $M_1 - M_2$ plane. We note here that for $\sin\theta_d < 0.1$, only co-annihilation can provide with right relic density, hence is independent of the choices $\sin\theta_d \sim 0.08$ or ~ 0.06 as has been chosen in Fig. 16.

5 Correlation between Dark and Neutrino Sectors

Following the discussion of the previous sections, we find that the observed value of nonzero θ_{13} and the Higgs portal coupling of a vector like dark matter can indeed be obtainable from a $U(1)$ flavor extension of

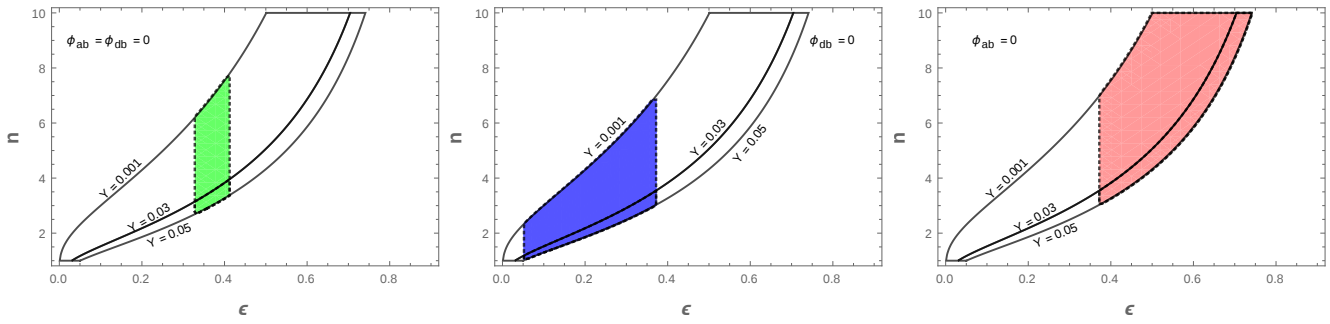

Figure 17: n vs ϵ to generate different values of $Y = \epsilon^n$ for (a) $\phi_{db} = \phi_{ab} = 0$ (left), (b) $\phi_{db} = 0$ (middle) and (c) $\phi_{ab} = 0$ (right).

the SM. In this section, we will see how θ_{13} measurement can affect the parameter space responsible for DM relic density. As discussed in section 3, θ_{13} is intimately related with the ϵ parameter as well as the phases $\phi_{ab,db}$ involved in the light neutrino mass matrix. The phase dependence can effectively be translated in terms of δ. Similarly from section 4, we find that the Yukawa coupling $Y = \epsilon^n$ is strongly constrained by the direct search of DM. We summarize here these constraints on ϵ and $Y = \epsilon^n$ to determine the unknown flavor charge n of the dark matter in our scenario. It is shown in Fig. 17. Colored patch in each plot corresponds to the allowed range of ϵ obtained in section 3 for Cases A,B,C and D. In the left panel of fig. 17, we have shown the allowed values of n where the CP-violating phases are taken to be zero corresponding to Case A. As the direct search of DM restricts the Y values to be $Y \lesssim 0.05$, we get $n \gtrsim 2$. Different contour lines with different Y values are shown in the figure. A similar conclusion holds for the other case (Case D) with $\phi_{db} = \phi_{ab} = \beta$. On the other hand, if $\phi_{ab} \neq \phi_{db}$ then a larger range of n values are expected to be allowed. In particular, by setting $\phi_{db} = 0$ and $\phi_{ab} \neq 0$ (as shown in middle panel of Fig. 17) we see that n can take any values starting from 1. On the other hand, if $\phi_{ab} = 0$ and $\phi_{db} \neq 0$ (as shown in the right panel of fig. 17) then n can take any values starting from 3. Thus the non-zero values of phases introduce more uncertainty in specifying n.

6 Conclusions

In this paper we have explored a $U(1)$ flavor extension of the SM to establish a possible correlation with the non-zero value of $\sin\theta_{13}$ with the relic abundance of dark matter. To start with we have shown a tri-bi-maximal mixing pattern of the neutrino mass matrix can be obtained from non abelian flavor symmetry, which results in $\sin\theta_{13} = 0$ in a basis where charged leptons are diagonal. In a simplest example, we can achieve the TBM structure of the neutrino mass matrix by assuming an $A_4 \times Z_3$ symmetry where the effective dimension six operators giving rise Majorana masses to neutrinos. The same symmetry also forbidden dimension five operators giving unwanted structure of neutrino mass matrix. We then augmented the SM with a dimension seven operator, allowed by the $U(1)$ flavor symmetry under which a dark sector consisting of vector-like fermions are charged. It is interesting to note that with the vector like fermions present in the dark sector, there exists a replica of SM Yukawa interaction in the dark sector. The $U(1)$ symmetry of the model was broken at a high scale by the vev of a flavon field ϕ to a remnant $\mathcal{Z}_2$ under which the dark sector particles were odd. As a result the lightest odd particles became a viable candidate of dark matter. Moreover, the dimension seven operator gave a correction to the TBM pattern of the neutrino mass matrix which predicted a non-zero value of $\sin\theta_{13}$. As a result we could show that the non-zero value $\sin\theta_{13}$ is proportional to the Higgs portal coupling, $Y = (\phi/\Lambda)^n \equiv \epsilon^n$, of the dark matter which gave rise correct relic density measured by WMAP and PLANCK and consistent with direct DM search bound from LUX. It is interesting to note that Y, on one hand is related to the mixing in the neutrino sector, while it

also crucially controlled by the mixing in the dark sector. We also found that the current allowed values of $\sin\theta_{13}$ gave the $U(1)$ charge of DM $\gtrsim 1$ which can be probed at the future direct DM search experiments such as Xenon-1T. The next to lightest stable particle (NLSP) is a charged fermion which can be searched at the LHC [17]. In the limit of small $\sin\theta_d$, the NLSP can give rise to a displaced vertex at LHC, a rather unique signature of the model discussed in ref. [16]. We argue that this is a minimal extension to SM to accommodate DM and non-zero $\sin\theta_{13}$ by using a flavor symmetric approach.

Acknowledgments

The work of SB is partially supported by DST INSPIRE grant no PHY/P/SUB/01 at IIT Guwahati. NS is partially supported by the Department of Science and Technology, Govt. of India under the financial Grant SR/FTP/PS-209/2011.

References

[1] S. Fukuda *et al.* [Super-Kamiokande Collaboration], Phys. Lett. B **539**, 179 (2002) [hep-ex/0205075]; Y. Ashie *et al.* [Super-Kamiokande Collaboration], Phys. Rev. D **71**, 112005 (2005) [hep-ex/0501064]. P. Adamson *et al.* [MINOS Collaboration], Phys. Rev. Lett. **106**, 181801 (2011) [arXiv:1103.0340 [hep-ex]]. T. Araki *et al.* [KamLAND Collaboration], Phys. Rev. Lett. **94**, 081801 (2005) [hep-ex/0406035].

[2] C. D. Froggatt and H. B. Nielsen, Nucl. Phys. B **147**, 277 (1979).

[3] E. Ma and G. Rajasekaran, Phys. Rev. D **64** (2001) 113012 [hep-ph/0106291].

[4] G. Altarelli and F. Feruglio, Nucl. Phys. B **741**, 215 (2006) [hep-ph/0512103].

[5] F. Capozzi, G. L. Fogli, E. Lisi, A. Marrone, D. Montanino and A. Palazzo, Phys. Rev. D **89**, no. 9, 093018 (2014) [arXiv:1312.2878 [hep-ph]].

[6] M. C. Gonzalez-Garcia, M. Maltoni and T. Schwetz, JHEP **1411**, 052 (2014) [arXiv:1409.5439 [hep-ph]].

[7] D. V. Forero, M. Tortola and J. W. F. Valle, Phys. Rev. D **90**, no. 9, 093006 (2014) [arXiv:1405.7540 [hep-ph]].

[8] Y. Abe *et al.* [Double Chooz Collaboration], Phys. Rev. Lett. **108**, 131801 (2012) [arXiv:1112.6353 [hep-ex]].

[9] F. P. An *et al.* [Daya Bay Collaboration], Phys. Rev. Lett. **108**, 171803 (2012) [arXiv:1203.1669 [hep-ex]].

[10] J. K. Ahn *et al.* [RENO Collaboration], Phys. Rev. Lett. **108**, 191802 (2012) [arXiv:1204.0626 [hep-ex]].

[11] K. Abe *et al.* [T2K Collaboration], Phys. Rev. Lett. **112**, 061802 (2014) [arXiv:1311.4750 [hep-ex]].

[12] G. Bertone, D. Hooper and J. Silk, Phys. Rept. 405, 279 (2005), arXiv:hep-ph/0404175.

[13] G. Hinshaw *et al.* [WMAP Collaboration], Astrophys. J. Suppl. **208**, 19 (2013) [arXiv:1212.5226 [astro-ph.CO]].

[14] P. A. R. Ade *et al.* **Planck Collaboration**, Astron. Astrophys. **571**, A16 (2014), arXiv:1303.5076 [astro-ph.CO].

[15] E. Aprile *et al.* [XENON Collaboration], [arXiv:1512.07501 [physics.ins-det]].

[16] S. Bhattacharya, N. Sahoo and N. Sahu, Phys. Rev. D **93**, no. 11, 115040 (2016) [arXiv:1510.02760 [hep-ph]].

[17] C. Arina, R. N. Mohapatra and N. Sahu, Phys. Lett. B **720** (2013) 130 [arXiv:1211.0435 [hep-ph]]; C. Arina, J. O. Gong and N. Sahu, Nucl. Phys. B **865**, 430 (2012) [arXiv:1206.0009 [hep-ph]].

[18] S. Bhattacharya, B. Karmakar, N. Sahu and A. Sil, Phys. Rev. D **93**, no. 11, 115041 (2016) [arXiv:1603.04776 [hep-ph]].

[19] P. F. Harrison, D. H. Perkins and W. G. Scott, Phys. Lett. B **458**, 79 (1999) [hep-ph/9904297].

[20] B. Karmakar and A. Sil, Phys. Rev. D **91**, 013004 (2015) [arXiv:1407.5826 [hep-ph]] and references there in.

[21] G. C. Branco, R. Gonzalez Felipe, F. R. Joaquim and H. Serodio, Phys. Rev. D **86**, 076008 (2012) [arXiv:1203.2646 [hep-ph]] and references there in.

[22] B. Karmakar and A. Sil, Phys. Rev. D **93**, no. 1, 013006 (2016) [arXiv:1509.07090 [hep-ph]].

[23] B. Karmakar and A. Sil, arXiv:1610.01909 [hep-ph].

[24] L. Calibbi, A. Crivellin and B. Zaldvar, Phys. Rev. D **92**, no. 1, 016004 (2015) [arXiv:1501.07268 [hep-ph]].

[25] M. Hirsch, S. Morisi, E. Peinado and J. W. F. Valle, Phys. Rev. D **82**, 116003 (2010) [arXiv:1007.0871 [hep-ph]]; W. C. Huang, JHEP **1411**, 083 (2014) doi:10.1007/JHEP11(2014)083 [arXiv:1405.5886 [hep-ph]]; I. de Medeiros Varzielas, O. Fischer and V. Maurer, JHEP **1508**, 080 (2015) [arXiv:1504.03955 [hep-ph]]; E. Ma, Phys. Lett. B **754**, 114 (2016) doi:10.1016/j.physletb.2016.01.033 [arXiv:1506.06658 [hep-ph]]; I. Medeiros Varzielas and O. Fischer, JHEP **1601**, 160 (2016) [arXiv:1512.00869 [hep-ph]]; A. Mukherjee and M. K. Das, Nucl. Phys. B **913**, 643 (2016) doi:10.1016/j.nuclphysb.2016.10.008 [arXiv:1512.02384 [hep-ph]]; J. M. Lamprea and E. Peinado, arXiv:1603.02190 [hep-ph].

[26] G. Altarelli and F. Feruglio, Rev. Mod. Phys. **82**, 2701 (2010) [arXiv:1002.0211 [hep-ph]].

[27] S. F. King and C. Luhn, JHEP **1109**, 042 (2011) [arXiv:1107.5332 [hep-ph]].

[28] K. Griest and D. Seckel, Phys. Rev. **D 43**, 3191 (1991); A. Chatterjee and N. Sahu, Phys. Rev. D **90**, no. 9, 095021 (2014) [arXiv:1407.3030 [hep-ph]].

[29] Y. Shimizu, M. Tanimoto and A. Watanabe, Prog. Theor. Phys. **126**, 81 (2011) [arXiv:1105.2929 [hep-ph]].

[30] K. A. Olive *et al.* [Particle Data Group Collaboration], Chin. Phys. C **38**, 090001 (2014).

[31] G. Cynolter and E. Lendvai, Eur. Phys. J. C **58**, 463 (2008) [arXiv:0804.4080 [hep-ph]].

[32] T. Cohen, J. Kearney, A. Pierce and D. Tucker-Smith, Phys. Rev. D **85**, 075003 (2012) [arXiv:1109.2604 [hep-ph]].

[33] C. Cheung and D. Sanford, JCAP **1402**, 011 (2014) [arXiv:1311.5896 [hep-ph]].

[34] G. Belanger, F. Boudjema, A. Pukhov and A. Semenov, Comput. Phys. Commun. **180**, 747 (2009) [arXiv:0803.2360 [hep-ph]].

[35] E. Aprile *et al.* [XENON100 Collaboration], Phys. Rev. Lett. **109**, 181301 (2012) [arXiv:1207.5988 [astro-ph.CO]].

[36] D. S. Akerib *et al.* [LUX Collaboration], Phys. Rev. Lett. **112**, 091303 (2014) [arXiv:1310.8214 [astro-ph.CO]].

[37] K.A. Olive et al. (Particle Data Group), Chin. Phys. C38, 090001 (2014) (URL: http://pdg.lbl.gov)

[38] P. A. R. Ade *et al.* [Planck Collaboration], arXiv:1303.5076 [astro-ph.CO].